

## Activities Report

Advanced training to the appointed MSc research fellow  
(March 21, 2022 to September 20, 2023)



Project: Predictive models for strategic metal rich, granite-related ore systems based on mineral and geochemical fingerprints and footprints

(FCT ERA-MIN/0005/2019 MOSTMEG)

<http://doi.org/10.54499/ERA-MIN/0005/2019>

Nuno Grácio

15 December, 2023



# 1 Introduction

The activities described in this report were performed by the grant holder within the MOSTMEG Project - *Predictive models for strategic metal rich, granite-related ore systems based on mineral and geochemical fingerprints and footprints*- ERA-MIN Joint Call 2019 (FCT ERA-MIN/0005/2019), from March 21, 2022 to September 20, 2023 (18 months) as required and predicted (Edital nº14 URMG, with extension of 4 months).

The activities were carried out in the scope of WP4 "Mineral Fingerprint and Footprints", Task 4.3 "*Reassessment of alluvial heavy minerals from old exploration surveys*", according to the work plan of the Research Grant (Edital nº14 URMG, and its extension). The focus was the mineralogical and chemical study of alluvial heavy minerals (HM) of the Segura region (Castelo Branco). The objectives of this task are to re-evaluate alluvial heavy minerals samples from former exploration surveys and find useful mineral pathfinders and fingerprints as a tool for Sn and W deposits exploration. As pointed in the MOSTMEG Transnational Proposal, the main goal of Task 4.3, *is the Re-examination of alluvial heavy minerals from old exploration surveys to evaluate the spatial extent of some mineral fingerprints/footprints and their usefulness in regional exploration strategies*. Moreover, in this sense, it is intended: (i) *the recognition and chemical characterization of mineral phases of higher relevance to the issues of interest among those forming the picked heavy mineral associations*. (ii) *the evaluation of the impact of potential mixing effects documenting signals from distinct sources (how should we process/filter them?)*; and (iii) *the relative abundance above which a certain mineral fingerprint or a given "proxy's assemblage" is reliable*. To reach the objectives, the minerals selected to be the focus in this study were the Sn-W ore minerals, i.e., cassiterite, wolframite, scheelite, TiO<sub>2</sub> polymorphs, i.e., rutile, anatase and brookite, and tourmaline; additionally, garnet raised interest for the study. The activities of the research grant were mainly performed at LNEG Alfragide facilities under the supervision of Dr. Rute Salgueiro [Principal Investigator (PI) in MOSTMEG FCT ERA-MIN/0005/2019]. Even so, as planned for this Task 4.3, there was scientific collaboration and support from Dr. Miguel Gaspar (Faculdade de Ciências da Universidade de Lisboa and IDL), Dr. Patrícia Moita, Dr. José Mirão, Dr. Mafalda Costa and Dr. André Cravinho (Universidade de Évora, Geociências - HERCULES), all-partner members of the Transnational MOSTMEG Project. This interconnection of activities materialized also in the follow-up of the grant holder in the chemical analysis of mineral samples by electron microprobe (EMP) at the FCUL facilities and by LA-ICP-MS at the Hércules facilities, and in

several (presential and online) meetings. Therefore, the results obtained, and its possible interpretation, until the date, presented here, include issues discussed with the PI and Task.4.3 team involved, and part was already presented and discussed in the 2<sup>nd</sup> and 3<sup>rd</sup> Annual Meeting, included in the 2<sup>nd</sup> and 3<sup>rd</sup> Annual Progress Report of the Transnational MOSTMEG Project and in the Short Activities Report (delivered with the Research Grant extension request). Additionally, the grant holder is co-author of a scientific paper published in the journal *Minerals* and an abstract presented in the XI Congresso Nacional de Geologia 2023.

## 1.1 Study area

The studied area is located in Segura (Castelo Branco), and it is included in the Central Iberian Zone (CIZ; Fig. 1). The main lithologies outcropping in this region encompass metasedimentary rocks belonging to the Slate- Greywacke Complex (SGC; Beiras Group: Malpica do Tejo Formation, upper and lower member; Neoproterozoic - Paleozoic), granitic rocks belonging to the Segura Massif (Portuguese part of the Cabeza De Araya Batholith outcropping in Spain; sin-tardi Variscan orogeny, 3rd phase: D<sub>3</sub>) and several types of mineralized veins (i.e., Sn-W Mineralized quartz veins; Sn-Li Mineralized aplite-pegmatite veins; W-Sn Mineralized quartz veins; Ba-Pb mineralized quartz veins) (Romão et al., 2010). The different mineral Sn-W/W-Sn and Li-Sn occurrences in the study area were part of, in the past, the Segura Mining Camp, which belongs to the tin-tungsten metallogenic belt of Góis-Segura. For the present study, Segura region was previously subdivided in 5 polygons (1 priority and 4 complementary areas dependent on the time and samples available to study), in the Portuguese territory, from which 2 were studied, (Fig. 1, Table 1). In the Polygon 1 (Segura mining region), the priority area to study, the large, zoned NW-SE elliptic granitic body, mentioned above, outcrops in the Southern part of this study area, produced a spotted-schist contact halo of about 500 m in the SGC rocks. Several barren veins (i.e. felsic, mafic and intermediate dykes, tonalitic porphyry and granodioritic porphyry dykes) also outcrop in this area. At approximately 1.5 km from the Polygon 2 (Southern region of Segura), towards Spain, outcrops the Estorninos intrusion (Variscan Age), a 7 km long porphyroid granitic body which also produces a metamorphic contact halo of about 600 m in the Spanish territory, as shown in Fig.1; however, according to Romão et al. (2010) this halo reaches the Erges river in the E-SE border of Polygon 2. In association with this intrusive body there is also the occurrence of a mineralized Sn vein on the northern part of its exocontact (in Spain; Fig. 1). Several other intrusive bodies outcrop in this polygon, namely quartz veins, lamprophyres and tonalite

porphyries (Romão et al., 2010). In both polygons, outcrops also Cenozoic sediments. The general structure of the region has a preferential WNW-ESE orientation, reflected in the folding of the metasediments of the Beiras Group, with WNW-ESE fold axes dipping to the SE, and a penetrative axial plane cleavage related to the 1st phase of Variscan deformation ( $D_1$ ) (Romão et al., 2010). The third phase of Variscan deformation ( $D_3$ ) in this region is characterized by its brittle behavior, resulting in the presence of dense fault networks (Romão et al., 2010). More recent episodes of deformation are associated with the Alpine cycle and correspond to reactivations of tectonic structures originated in the Variscan orogeny (Romão et al., 2010).

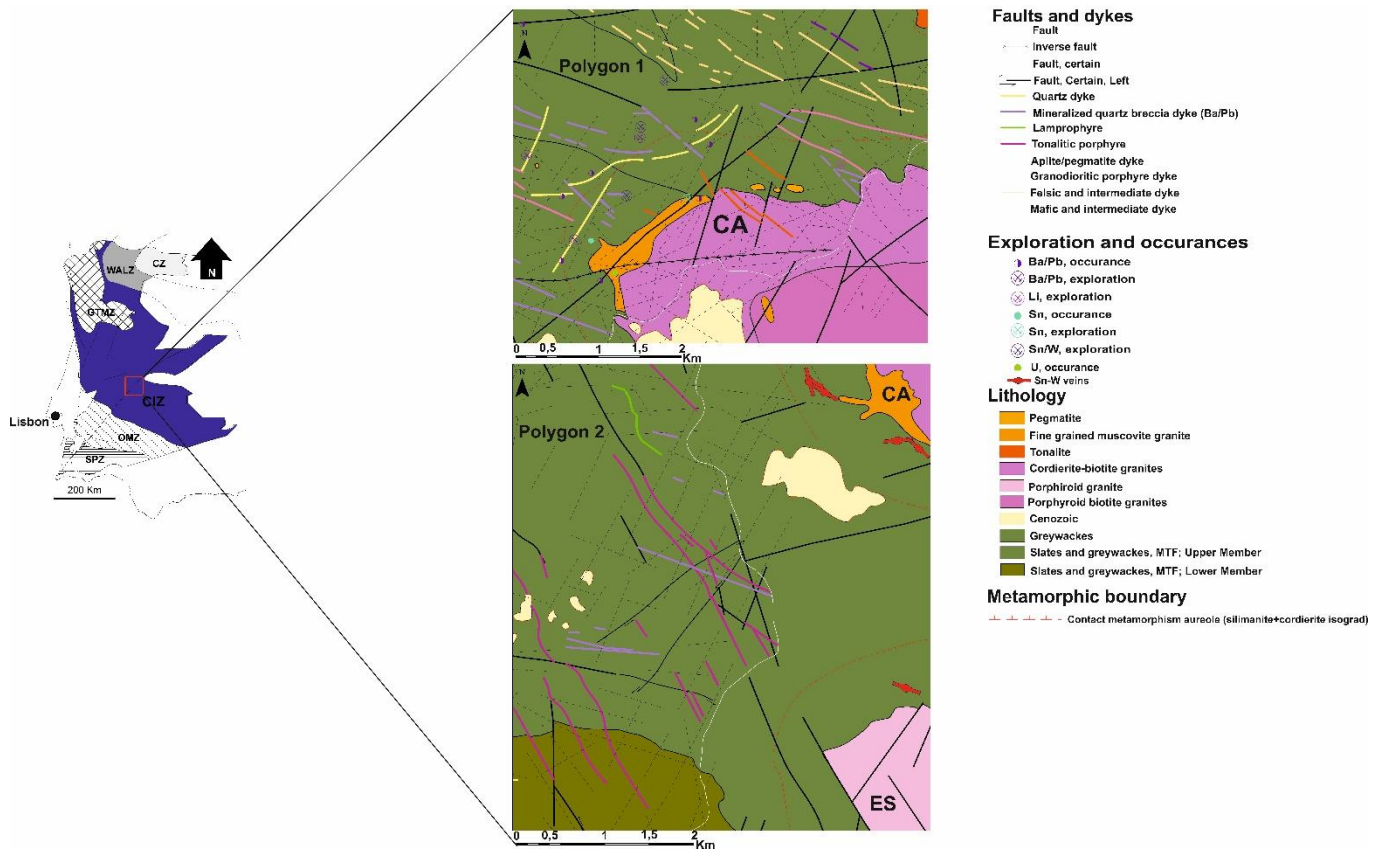


Fig. 1 – Localization of the study area and its geological setting: Segura Mining region (Polygon 1); and Southern region of Segura (only in Portuguese territory; Polygon 2); plotted in an extract of the geological map produced by the MOSTMEG transnational project team. ES – Estorninos Granite; CA – Cabeza de Araya batholith. Additional data about the Sn occurrences in the Spanish territory were adapted from Mapa metalogenético de la provincia de Cáceres. Escala 1:200 000. IGME.

## 2. Summary and methodologies of the work developed

### 2.1. Mineralogical analysis

Under the framework of the Task 4.3 (WP4) and its objectives, alluvial heavy minerals present in (47) samples from Polygon 1 and (28) samples from Polygon 2 have been identified and characterized under binocular microscope (Fig. 2, Table 1) by the grant holder, according to the work plan. It is important to note that, for MOSTMEG research, the reassessment of the alluvial samples studied from LNEG old surveys included 69 samples from Polygon 1 (1a: 34 samples ; 1b: 35 samples), and 35 from Polygon 2 (Fig. 2; Table 1); and some samples from Polygon 1 were also studied after Gracio (2020) (i.e. 5) or samples data from this study were used (i.e. 43 samples; Fig. 2a).

In this first stage the minerals were semi-quantified according with the range table: < 1 %; 1 to 5 %; 5 to 25 %; 25 to 50 %; 50 to 75 %; 75 to 100%, adapted from Parfenoff et al. (1970; with an error of 5%) and where the percentage of the mineral quantified is relative to the volume of the respective mineral fraction (i.e. magnetic or non-magnetic).

Along this study stage, it was used the UV light for scheelite identification/characterization and tinning test for cassiterite identification (adapted from Parfenoff et al., 1970) in several samples; in cases, where the cassiterite grains were tinned, it was necessary to reverse the tinning process by embedding the non-magnetic fraction of the sample in hydrochloric acid (in these cases, to prevent eventual chemical reactions with possible alloying elements in the border of gold (alloy) grains, these grains were removed); also, the hand magnet helped to differentiate some mineral grains and, along with the work development, microphotographs were taken.

To verify their suitability in mineral exploration works, physical properties (e.g., color, habit, size, pleochroism, zonation and inclusions) of the cassiterite, wolframite, scheelite, TiO<sub>2</sub> polymorphs and additionally tourmaline and garnet were analyzed using a binocular microscope, as initially implemented by the Principal Investigator (PI; MOSTMEG Project, part LNEG) in the first 22 studied samples from Polygon 1. The grant holder has collaborated with the PI in the development of this methodology and several mineral populations of cassiterite, tourmaline, rutile, anatase, brookite and garnet according to their physical properties were identified and characterized and mineral standards for these populations were made to serve as a guide for the mineralogical survey. For wolframite and scheelite nonrelevant different population were discriminated. The experimental study of the

percentage of each mineral population was also made, although the difficulty of this task was greater than for mineral phases, due to the difficult distinction between the properties of all the grains from the different mineral populations identified, given the large number of mineral grains available in each sample (in many cases in the order of thousands). Nonetheless, for this propose, the same semi-quantification table range mentioned above (< 1 %; 1 to 5 %, 5 to 25 %; 25 to 50 %; 50 to 75 %; 75 to 100%) was used considering the average values, as for the mineral phases.

*Table 1 – Geological setting of the different polygons of the study area with the number of samples studied and used in maps production, and mineral mounts produced with mineral grains from each one. The alluvial samples studied from LNEG old surveys included 69 samples from Polygon 1 and 35 from Polygon 2; some samples from Polygon 1 were also re-analyzed (i.e. 5 samples), or their data was used (i.e. 43 samples) from Grácio (2020).*

<b>Polygon</b>	<b>Geological Setting</b>	<b>Nº alluvial samples of heavy mineral concentrates studied: by the MSc research fellow / (total)</b>	<b>N.º samples used for Mineral distribution maps</b>	<b>Mounts</b>
<b>1a</b>	Segura granite distal/proximal exocontact, granitic porphyry, mineralized quartz breccia, quartz and aplite-pegmatitic veins hosted in SGC rocks	15 / (34) (5 after Grácio (2020))	34 + 27 (MOSTMEG + Grácio, 2020)	ANA1, CASS1, CASS2, CASS6, RUT1, SCH1, Wif1, GRT1, TUR1
<b>1b</b>	Segura granite proximal exocontact, granitic porphyry, mineralized quartz breccia, quartz and aplite-pegmatitic veins hosted in SGC rocks	32 / (35)	35+16 (MOSTMEG + Grácio, 2020)	RUT2, ANA2, CASS3, CASS4, SCH1, WLF1, GRT2, TUR2
<b>2</b>	Lamprophyres, tonalitic porphyry, quartz and mineralized quartz breccia veins hosted in SGC rocks, around Estorninos granite exocontact	28 / (35)	35	ANA3, CASS5, CASS6, RUT3, SCH2

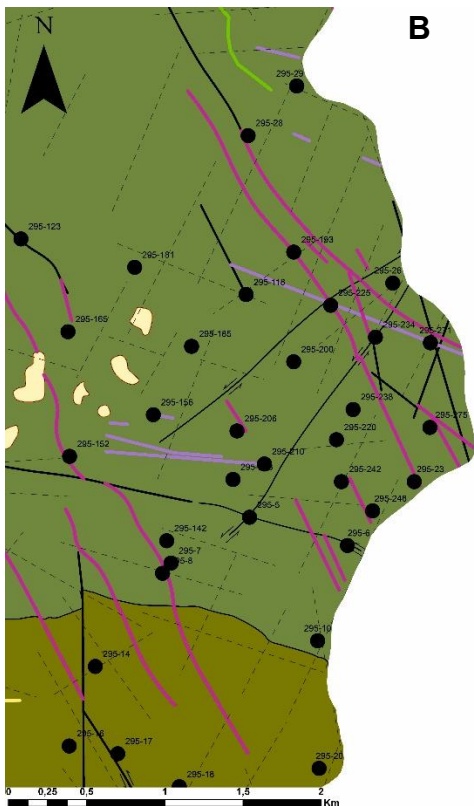
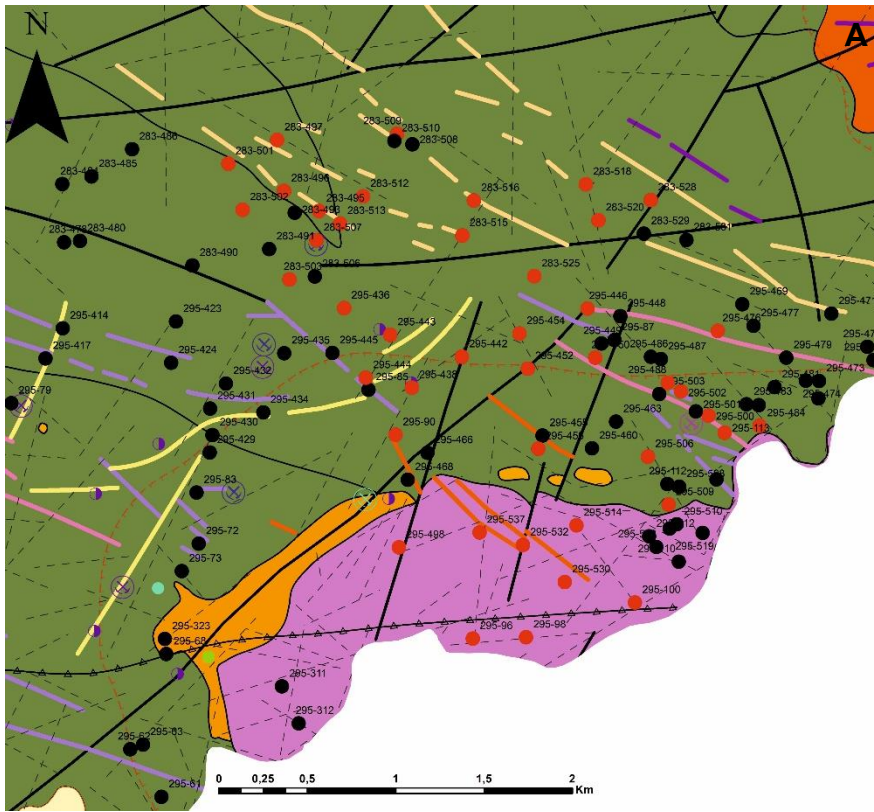


Fig. 2 - A) Location of the 69 alluvial samples from the Polygon 1 studied in MOSTMEG: black dots; Location of the additional 43 alluvial samples from Grácio (2020): red dots. B) Location of the 35 alluvial samples from the Polygon 2 studied in MOSTMEG.

## 2.2. Processing data

After identification, semi-quantitative analysis and statistical study of the different mineral species, the average percentage (relative to the total volume of the sample, i.e. the volume of the magnetic + non-magnetic mineral fraction), in the total volume of the 69 samples of alluvial heavy minerals from Polygon 1 (Table 4) and 35 from Polygon 2 (Table 5) were determined with the aid of a specialized excel spreadsheet, considering the average values of the table range mentioned above in section 2.1 (that is, the average total percentage for each sample).

For Polygon 1, after data processing in specialized excel spreadsheet, the average abundance of the mineral assemblage in six studied samples were selected as representative of the (main) mineral contribution from different geological sources to alluviums in this area, i.e. Segura granite, SGC metasediments, Sn-W / W-Sn mineralized quartz veins, Sn-Li mineralized aplite-pegmatite veins and Ba-Pb mineralized quartz veins (Fig. 3).

The number of cassiterite, scheelite and wolframite grains from previous studies of LNEG old surveys for the 1044 samples in the region that includes all the defined polygons were used to produce the mineral grains distribution maps during the previous MOSTMEG (WP1) activities. An update and refinement of these maps was made by the grant holder, in an ArcGIS software database, by including the region around Polygon 1 and 2 (647 samples) together and updating the Polygon 2 wolframite data (after the heavy minerals analysis: 6 grains were identified in sample 295-200) (Fig. 4).

After the semi-quantification of the different minerals and the cassiterite, rutile, anatase, brookite, tourmaline and garnet populations (identified according to their physical properties), the data for each mineral (average abundance, population types, population type abundance) was inserted in an ArcGIS software database and the six respective maps were produced, one for each mentioned above mineral (Fig. 5 and 6). In the set of six maps present in Fig. 6 the size of the slices in each pie chart (markers) represents the abundance of each population identified in that sample in relation with the other populations. To obtain this value for each mineral population, it was considered the average abundance of each mineral in the sample (calculated as described above) as 100% and then calculate the abundance of each population type identified and semi-quantified (according to the range table)

considering its average value. The same process was applied for the samples in the polygon 2 (Fig. 8 and Fig. 9).

To strengthen the data of the mineral distribution maps, on the Polygon 1, the average percentage of the selected minerals for MOSTMEG research in the 43 samples from Grácio (2020; Fig. 2A) study was also used. The values of the average ratios of cassiterite, wolframite, scheelite, TiO<sub>2</sub> polymorphs and garnet from a total of 112 (69 + 43) samples were projected onto geological maps allowing the visualization of the distribution of these minerals in the study area and their relation to proximal geological features (Fig. 11). For the Polygon 2 the same method was used with the values from the 35 samples studied (Fig. 12).

Regarding the chemical data, comprehensive EMP and LA-ICP-MS analyses were conducted and organized into distinct Excel spreadsheets, each dedicated to a specific mineral specimen. Subsequently, the processed chemical data was used to craft informative graphical representations, unveiling specific nuances within the trace element compositions of the analyzed minerals, thus furnishing some insights to guide future research endeavors. Notably, Ternary diagrams, instrumental to show different compositions for titanium polymorphs, were constructed using the TriDraw software (Fig. 13 and Fig. 16), while Python was employed to generate visually Violin plots for the graphical representation of the composition of the various cassiterite types identified (Fig. 14).

## **2.3 Preparation of mineral mounts for chemical analysis**

The separation and handpicking of a total of 1363 and 506 grains of anatase, rutile, cassiterite, tourmaline, wolframite, scheelite additionally garnet and some ilmenite grains for testing, from different samples of Polygon 1 and Polygon 2, respectively, representing different populations, was carried out with the objective of analyzing these grains using electron microprobe (1136 analyses) and LA-ICP-MS (570 analyses performed by FCUL and UE partners) (Table 2). Therefore, 19 mineral mounts were made with a mixture of epoxy resin and a hardener, left to dry for 24 hours, and then polished to be able to analyze these grains (Tables 2 and 3).

Table 2 - General information about the mineral mounts produced in this project.

Mount	Minerals	N° samples	N° grains	N° analyses (EMP)
ANA1	Anatase	7	101	209 + 234 (EMP + LA-ICP-MS-Evora partner)
ANA2	Anatase	9	91	
ANA3	Anatase	11	107	
CASS1	Cassiterite (Rutile)	8	81(5)	250 (9)
CASS2	Cassiterite (Rutile)	7	103 (2)	185 (6)
CASS3	Cassiterite (Rutile?)	7	74	53 (LA-ICP-MS Evora Partner)
CASS4	Cassiterite (Rutile?)	10	72	49 (LA-ICP-MS Evora Partner)
CASS5	Cassiterite	11	101	
CASS6	Cassiterite	8	128	
GRT1	Garnet (+ Ilmenite grains)	11	38(23)	130 (68)
GRT2	Garnet	15	102	
RUT1	Rutile	7	105	
RUT2	Rutile	11	84	
RUT3	Rutile	10	116	
SCH1	Scheelite	15	97	
SCH2	Scheelite	9	89	
TUR1	Tourmaline	11	142	279 + 234 (EMP + LA-ICP-MS; FCUL partner)
TUR2	Tourmaline	11	107	
WLF1	Wolframite	14	101	

Table 3 - Samples from which the grains of each mounts were collected.

Mount	Samples
ANA1	283-478; 283-510; 295-62; 295-73; 295-85; 295-424; 295-468
ANA2	295-87; 295-116; 295-448; 295-463; 295-469; 295-472; 295-486; 295-501; 295-519
ANA3	295-8, 295-10, 295-14, 295-17, 295-118, 295-181, 295-185, 295-206, 295-234, 295-238, 295-246
CASS1	283-478; 283-510; 295-63; 295-73; 295-85; 295-423; 295-423; 295-431; 295-468; 295-468
CASS2	283-485; 295-68; 295-83; 295-445; 283-506; 295-414
CASS3	283-485; 283-506; 295-68; 295-83; 295-414; 295-445
CASS4	295-87; 295-110; 295-115; 295-449; 295-471; 295-486; 295-503; 295-508; 295-510; 295-519
CASS5	295-7, 295-17, 295-28, 295-118, 295-123, 295-152, 295-156, 295-193, 295-201, 295-210, 295-220
CASS6	283-491, 283-493, 295-5, 295-6, 295-10, 295-23, 295-220, 295-246
GRT1	283-484; 283-508; 295-63; 295-63; 295-72; 295-311; 295-312; 295-323; 295-423; 295-429; 295-434; 295-435
GRT2	283-484; 295-61; 295-87; 295-110; 295-414; 295-429; 295-435; 295-460; 295-472; 295-483; 295-490; 295-511; 295-513; 295-519
RUT1	283-478; 283-506; 295-79; 295-312; 295-323; 295-430; 295-435
RUT2	295-110; 295-449; 295-460; 295-469; 295-471; 295-479; 295-488; 295-508; 295-510; 295-540
RUT3	295-5; 295-16; 295-29; 295-123; 295-156; 295-185; 295-210; 295-225; 295-246; 295-271
SCH1	283-491; 295-63; 295-115; 295-414; 295-448; 295-455; 295-466; 295-468; 295-472; 295-477; 295-482; 295-501; 295-471; 295-417; 295-510
SCH2	295-6; 295-7; 295-10; 295-20; 295-23; 295-210; 295-220; 295-246; 295-271
TUR1	283-484; 283-490; 283-508; 283-510; 295-63; 295-72; 295-83; 295-323; 295-430; 295-435; 295-468
TUR2	295-460; 295-471; 295-472; 295-479; 295-483; 295-487; 295-490; 295-503; 295-508; 295-511; 295-519
WLF1	283-478; 283-490; 283-493; 283-506; 283-510; 295-61; 295-73; 295-79; 295-85; 295-424; 295-449; 295-463; 295-510

## **2.4 Chemical analysis**

The 1136 EMP and 570 of LA-ICP-MS analysis were performed most of which with the grant holder monitorization, and with the coordination and assistance of FCUL and UE partner, in FCUL and Hércules facilities (Table 2). The EMP chemical data organization and processing, in excel, of all the minerals analyzed except for the garnets (by FCUL partner) was conducted by the grant holder. LA-ICP-MS data was processed and organized by the UE partner and the data was then used to produce diagrams and graphs by the grant holder. Cassiterite grain images by cathode-luminescence (CL) were also obtained to define the more adequate zones to be analyzed by EMP, these images were performed in the Hércules laboratory (Universidade de Évora partner). The grant holder has updated the data treatment of the LA-ICP-MS tourmaline analysis (original data treatment interpretation performed by the FCUL partner) discriminating the different tourmaline population types. The chemical data generated were organized in different excel sheets for each mineral, and each analysis point is controlled (this means that in this geochemical database there is also the information about the type of grain, from which sample, if the analysis was made in the core or border of the mineral grain, if the grain is zoned, the mount that it corresponds to the row, the number of the grain from that row and from which population type the grain is, if applicable). This data was then used to produce different geochemical discriminant diagrams for the different minerals (cassiterite, rutile, anatase, tourmaline and garnet) to aid and present T. 4.3 team interpretations.

## **3. Results**

### **3.1 Heavy Mineral Analysis**

In Table 4 are represented all the 33 minerals phases s.l., in addition to iron-oxi/hydroxides, undifferentiated minerals or sulphides and the discrimination of altered pyrite, during the heavy mineral analysis and their average percentage in the total of the 69 samples of the Polygon 1; and in Table 5 are represented the 23 minerals phases s.l., plus iron-oxi/hydroxides and undifferentiated minerals in addition to the discrimination of altered pyrite during the heavy mineral analysis and their average percentage in the total of the 35 samples studied of the Polygon 2.

The abundance (average %) of the iron oxides-hydroxides (58.23 % - Polygon 1; 66.95 % - Polygon 2) stands out from the remaining minerals since they are present in practically all the samples and, generally, in significant quantities, while the remaining minerals, although with lower average %, can be quite abundant in some samples. Of the minerals of interest for the present study, and regarding Sn and W ore minerals, cassiterite is more abundant than wolframite and scheelite (i.e. 6.31 % - Polygon 1; 4.63 % - Polygon 2) in both Polygons; and regarding the W ore minerals wolframite is the most abundant in the Polygon 1 (1.51 % - Polygon 1; 0.03 % - Polygon 2); however in the Polygon 2 scheelite is the dominant W ore mineral (0.42 % - Polygon 1; 1.10 % - Polygon 2).

The tourmaline abundance in Polygon 1 is high (5.41%) due to the samples in the Segura granite, which are very abundant in tourmaline due to the presence of this mineral in those rocks; in the Polygon 2 the abundance of tourmaline is not as great (3.61%), but it is still one of the most common heavy minerals found on those samples. Garnet behaves similarly as tourmaline, although with lower abundances, the higher percentage of garnet in the Polygon 1 (0.55%) is due to the samples in the Segura granite having a lot more garnet grains than those outside of the granite, and in the Polygon 2 area where there is no granite outcrop, the abundance of this mineral drops (0.06%). Anatase is the most common titanium polymorph found on the samples of the Polygon 1 and 2 (2.95 % - Polygon 1; 1.66% - Polygon 2), followed by rutile (0.68 % - Polygon 1; 0.52 % - Polygon 2) and brookite is the least abundant titanium polymorph (0.28 % - Polygon 1; 0.07 % - Polygon 2).

In some samples on both polygons, composite grains of fine tourmaline aggregates were identified associated with cassiterite or phyllosilicates. These tourmaline needles could indicate tourmalinization processes affecting the SGC rocks or the mineralized veins, in cases suggesting close association with cassiterite deposition. Additionally, undifferentiated sulphides grains and a few fresh sulphides, namely galena, chalcopyrite, and pyrite grains, were detected. Given their susceptibility to surface weathering, their presence may imply proximity to their source.

Table 4 - Average percentage of each mineral in the total volume of the 69 samples of alluvial heavy minerals from the Polygon 1 of the Segura mining region. MGN-magnetic minerals fraction; NM-nonmagnetic minerals fraction.

Mineral	% Average	Mineral	% Average	Mineral	% Average
Iron oxides-hydroxides	58.23	Topaz	00.46	Xenotime	0.02
Ilmenite	11.98	Scheelite	0.42	Pyrite	0.01
Cassiterite	6.31	Leucoxene (MGN)	0.41	Staurolite	0.01
Tourmaline	5.41	Brookite	0.28	Galena	0.01
Baryte	3.89	Andalusite	0.27	Sillimanite	0.01
Anatase	2.95	Alt. Pyrite	0.22	Epidote	0.01
Wolframite	1.51	Gold	0.09	Monazite	0.01
Leucoxene (NM)	1.16	Muscovite	0.08	Kyanite	<0.01
Apatite	1.13	Siderite	0.05	Chalcopyrite	<0.01
Rutile	0.68	Cinnabar	0.04	Undifferentiated minerals	2.64
Garnet	0.55	Columbo-Tantalite	0.02		
Zircon	0.54	Chlorite	0.02		
Biotite	0.51	Undifferentiated	0.02		
		Sulphides			
<b>Total</b>					<b>100.00</b>

Table 5 - Average percentage of each mineral in the total of the 35 samples of alluvial heavy minerals from the Polygon 2 of the Segura mining region. MGN-magnetic minerals fraction; NM-nonmagnetic minerals fraction.

Mineral	% Average	Mineral	% Average
Iron oxides-hydroxides	66.95	Garnet	0.06
Ilmenite	15.5	Chalcopyrite	0.03
Cassiterite	4.63	Gold	0.03
Tourmaline	3.61	Cinnabar	0.03
Zircon	2.70	Biotite	0.03
Anatase	1.66	Wolframite	0.03
Scheelite	1.10	Pyrite	0.01
Baryte	0.68	Topaz	0.01
Alt. Pyrite	0.56	Muscovite	0.01
Rutile	0.52	Galena	0.01
Andalusite	0.26	Sillimanite	<0.01
Leucoxene (NM)	0.14	Apatite	<0.01
Brookite	0.07	Undifferentiated minerals	1.88
<b>Total</b>			<b>100.00</b>

Regarding the distinction of mineral grains, several mineral populations of cassiterite (i.e. 9; according to their: color and pleochroism, habit, zoning/banding, luster, inclusions/associated minerals and grains

size), tourmaline (i.e. 7; according to their: color, pleochroism, habit, inclusions, zoning and grain size), rutile (i.e. 7 population types, according to their color, diaphaneity, habit, zoning and grain size and subdivided in 4 population groups), anatase, brookite and garnet (2 population types, according to their: color, diaphaneity, habit, zoning and grain size) were identified and semi-quantified during the study under binocular microscope; the results of the semi-quantification experimental study are presented graphically in section 3.2.2 (Fig. 6 and 9).

It was also possible to observe that the heavy mineral associations identified mostly reflect the outcropping lithologies of their sampling location, including specific evidence of different types of mineralization. The mineral association of six samples chosen to exemplify this relation are represented in Fig. 3; In general, the samples collected in the area where the Segura Massif outcrops (e.g. 295-312; Fig. 3A) typically show abundant tourmaline and frequently some garnet, biotite, muscovite and rutile; the presence of barite can be justified by the strong association of the Ba-Pb ore veins and granitic rocks. For the samples collected in the drainage areas where the SCG rocks outcrop (e.g. 283-486; Fig. 3B), without direct influence of igneous or hydrothermal bodies, mostly have iron oxides-hydroxides and altered minerals (leucoxenes). In samples collected in the proximal zones of Sn-W/Li-Sn, Ba-Pb ore veins and dykes it is common to find samples with relatively higher abundances of cassiterite (e.g. 295-432; Fig. 3C) wolframite (e.g. 283-506; Fig. 3D) and, in the last case, baryte (e.g. 295-79; Fig. 3F), depending on the type or types of proximal mineralization (Fig. 2).

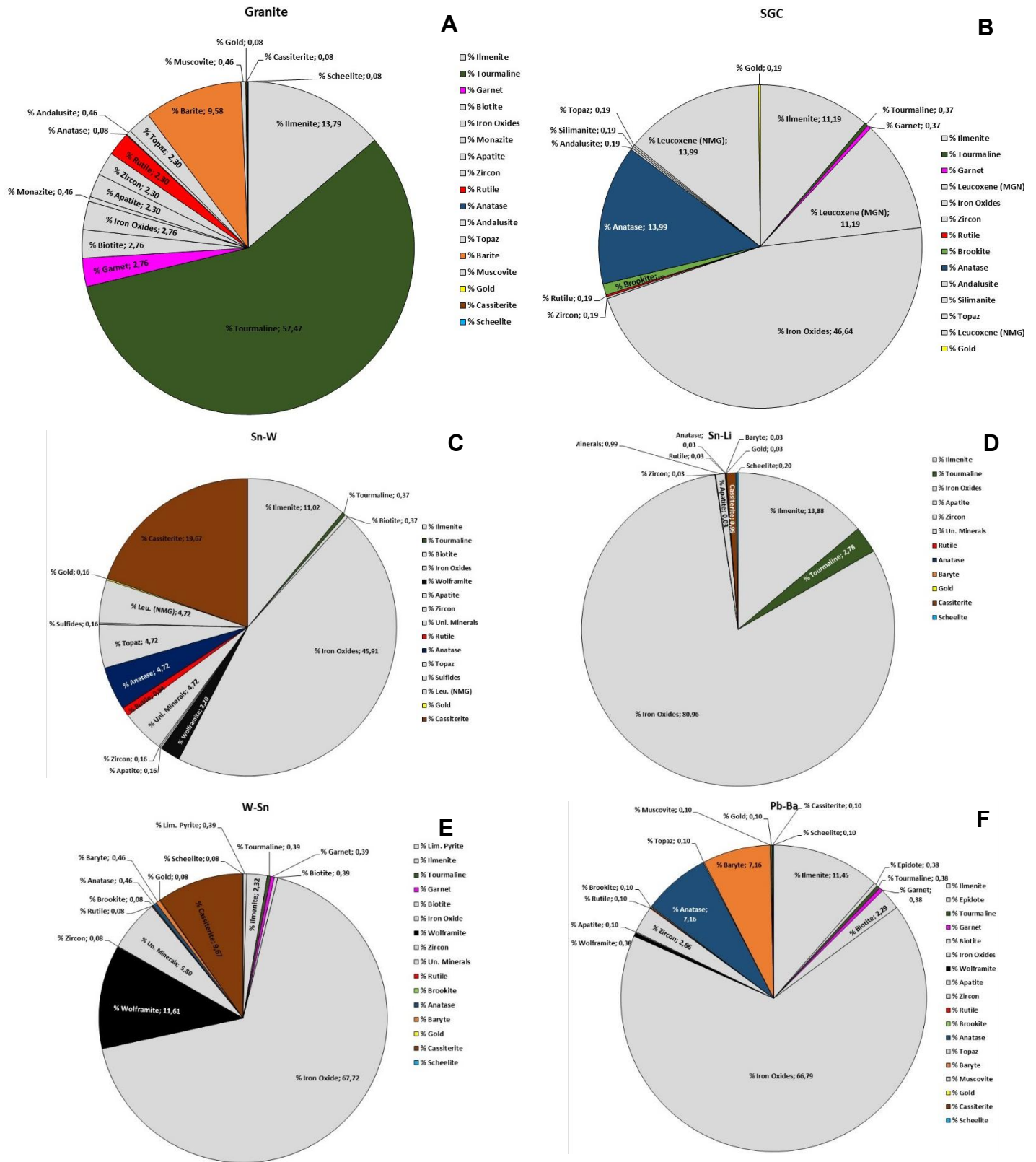


Fig. 3- Pie charts of six samples representing examples of alluvial heavy minerals of the Segura mining region (Polygon 1) collected in areas under the influence of the mineral contribution from specific lithologies to alluviums: A) 295-312 – Segura Granites; B) 283-486 – SGC Metasediments; C) 295-432 – Sn-W Mineralized quartz veins; D) 295-503 – Sn-Li Mineralized aplite-pegmatite veins; E) 283-506 – W-Sn Mineralized quartz veins; F) 295-79 – Ba-Pb mineralized quartz veins.

## 3.2 Heavy Minerals Regional Distribution

### 3.2.1 Mineral grains abundance maps

As mentioned in section 2,2, an update of the maps of the abundance of grains was made as concern to the number of grains scale and in one sample (295-200) where no wolframite was previously identified, 6 grains were identified and added to the database, these maps were also updated to include the polygon 2 area (Fig. 4). The update obviously confirms the localization of the mineral anomalies in close association with the mineralizations around granitic intrusions, as previously identified and described in the MOSTMEG annual reports; however, the displayed information is now better exposed.

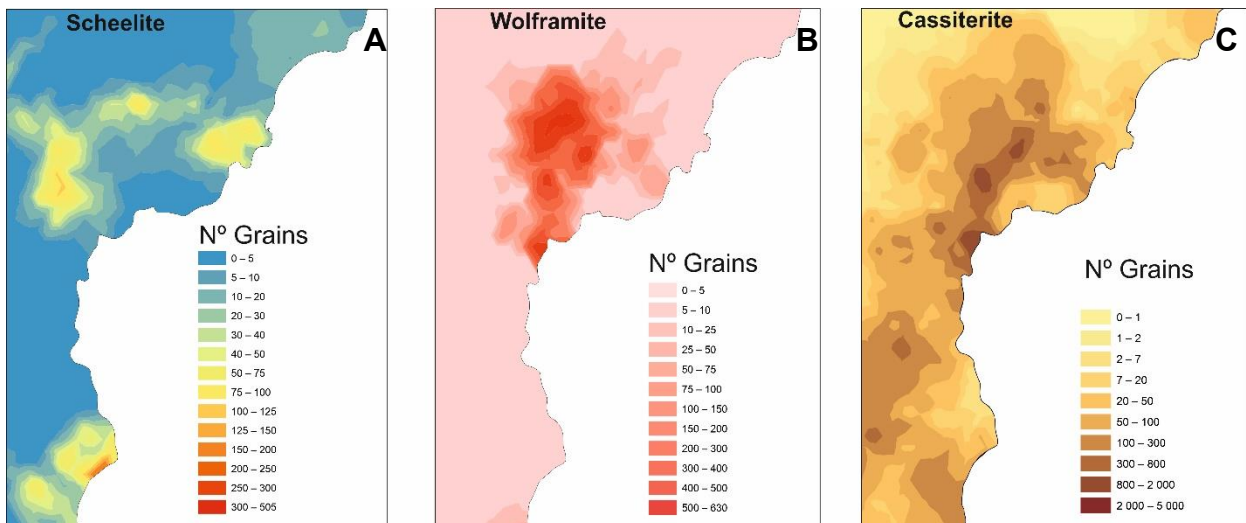


Fig. 4 – Maps of the abundance by the total number of grains of A) Scheelite; B) Wolframite; C) Cassiterite of the 647 samples from old surveys in which are included the samples from Polygon 1 and 2 area that were study under the MOSTMEG research.

### 3.2.2 Mineral population maps

In this section are presented the maps of the distribution of the different cassiterite, rutile, anatase, brookite, tourmaline and garnet populations identified and semi-quantified in the Polygon 1 and 2 as well as the maps of the samples where tourmaline aggregate grains and sulfides were identified.

#### 3.2.2.1 Polygon 1

The Fig. 5 presents the map of different mineral populations identified in the heavy mineral samples of the Polygon 1, and the Fig. 6 presents the map of the relative abundance percentage of those mineral populations. As can be seen, cassiterite, tourmaline and rutile populations are more variable in the W

side than in the E side samples of the study area (Fig. 5). We can also observe that some mineral populations are more abundant in one side than the other, for example: cassiterite grains from Type 3 are more abundant in the W side and the Type 2 grains are more abundant in the E side; the garnet grains from the Type 2 (almandine garnets) are usually more abundant in the samples collected where or near the Segura granite outcrops, whereas the Type 1 garnet grains (spessartine) are more abundant in the samples collected in the exocontact of this massif); however, there is an alignment of samples with some (although few) Type 2 garnet grains away from known granite outcrops; there are cluster of samples in the NW limit of the polygon, near different mineralized structures of different natures, where the Group A rutile grains are the most abundant population. As for anatase and brookite populations, Type 1 are predominant in the study area for both minerals.

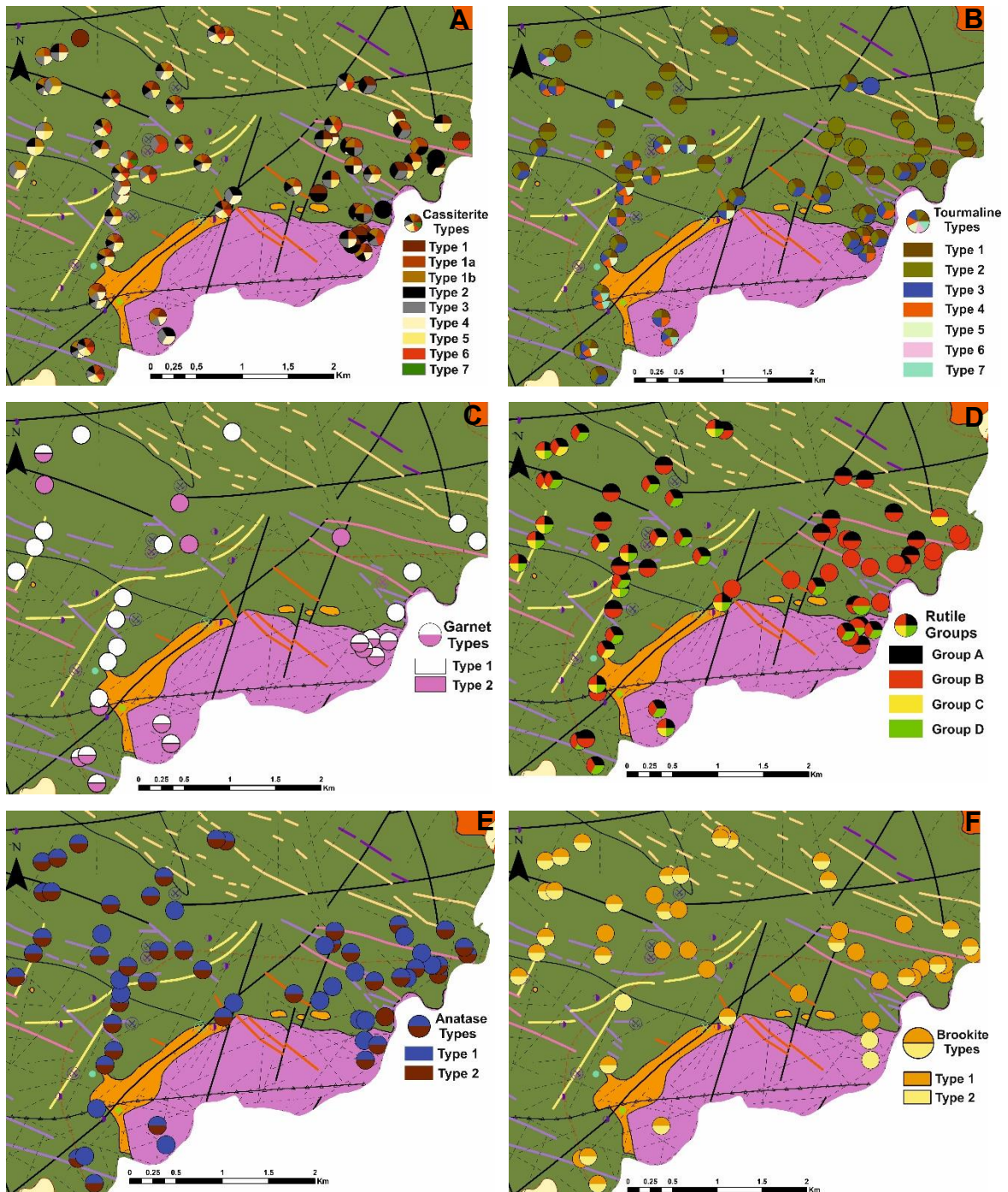


Fig. 5 - Maps of the regional distribution of mineral populations for Polygon 1 samples (experimental study of 69 alluvial samples;) projected on an extract of the MOSTMEG geological map. Grain populations for: A) Cassiterite, defined mainly by color, diaphaneity and pleochroism; B) Tourmaline, defined by color similar to legend markers; C) Garnet (defined by physical and chemical properties: Type 1: spessartine; Type 2: almandine); D) Rutile, defined by habit (Group A: prismatic; Group B: anhedral; Group C: acicular polycrystalline aggregates; Group D: bipyramidal and others undifferentiated); E) Anatase, defined by habit (Type 1: bipyramidal; Type 2: basal); F) Brookite, defined by color.

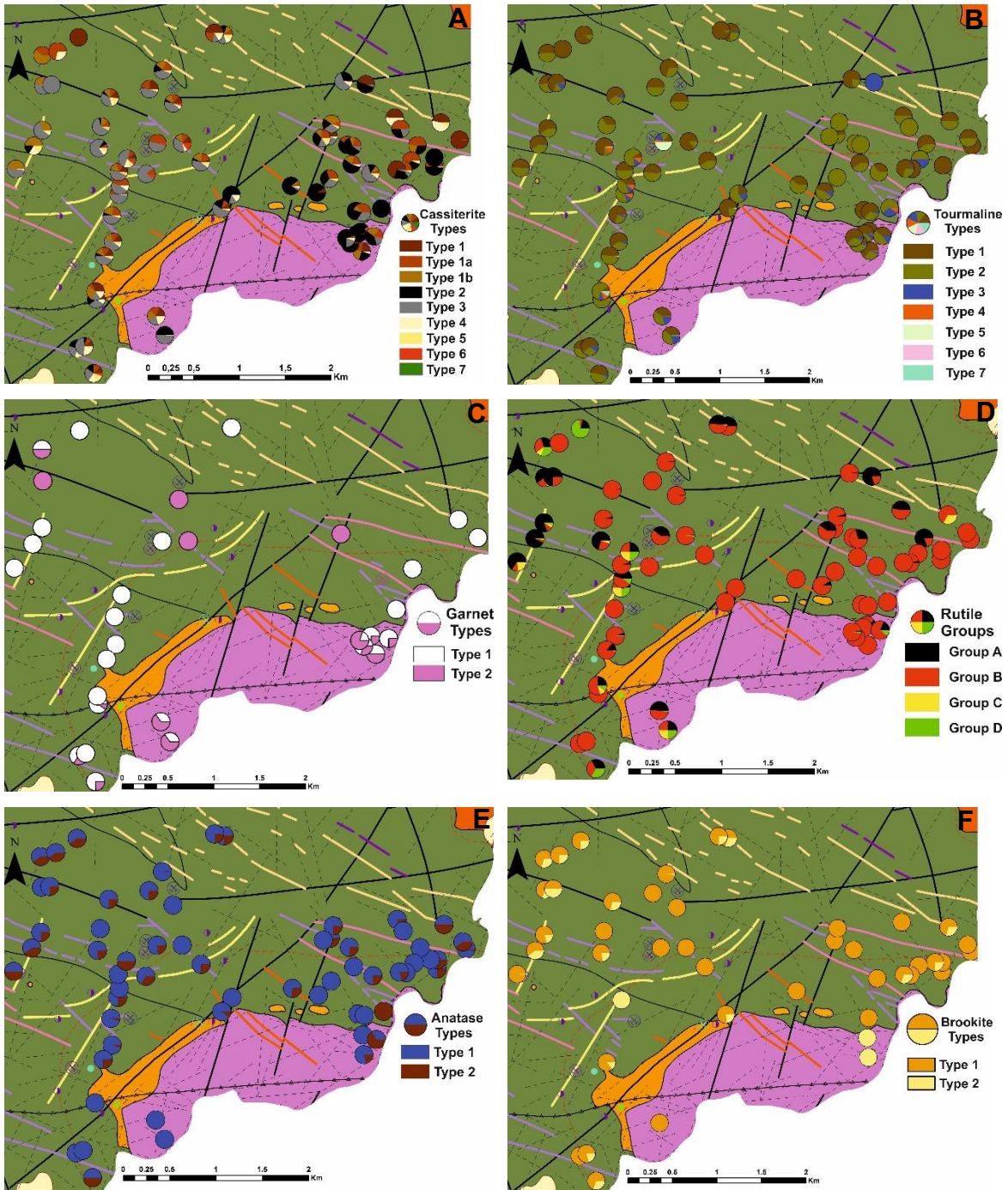
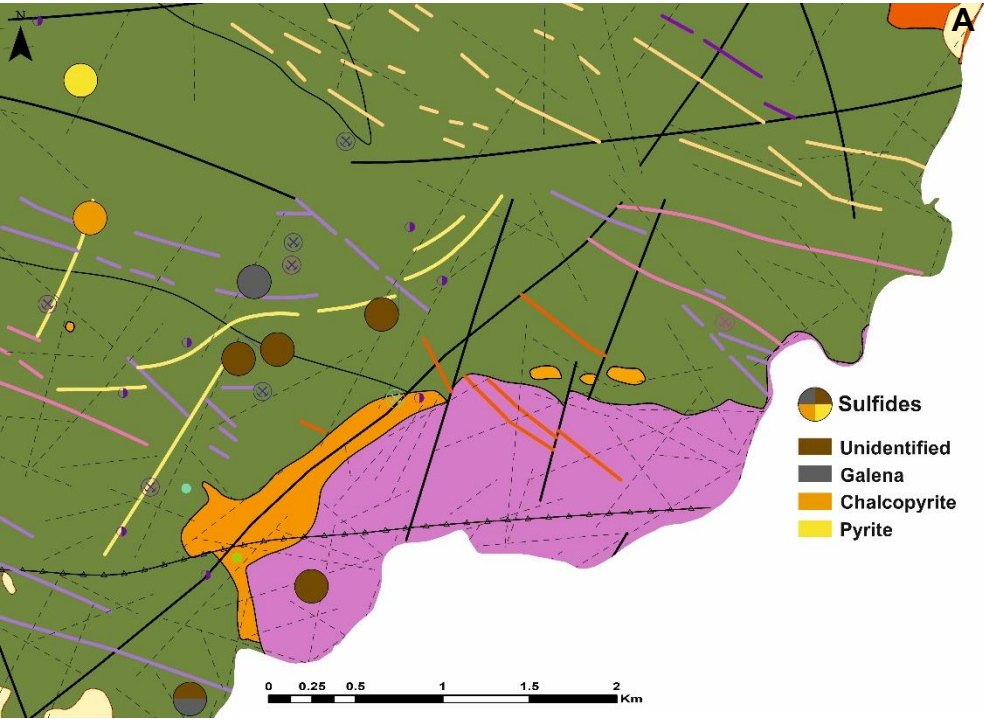


Fig. 6 - Maps of the relative abundance of mineral populations for Polygon 1 samples (experimental study of 69 alluvial samples;) projected on an extract of the MOSTMEG geological map. Grain populations for: A) Cassiterite, defined mainly by color, diaphaneity and pleochroism; B) Tourmaline, defined by color similar to legend markers; C) Garnet (defined by physical and chemical properties: Type 1: spessartine; Type 2: almandine); D) Rutile, defined by habit (Group A: prismatic; Group B: anhedral; Group C: acicular polycrystalline aggregates; Group D: bipyramidal and others undifferentiated); E) Anatase, defined by habit (Type 1: bipyramidal; Type 2: basal); F) Brookite, defined by color.

The sulphides identified in some samples, are located where the bulk of the old mining works were present, particularly in the samples from the W zone of the Polygon 1 (Fig. 7A).

The regional distribution map of the composite grains of fine tourmaline aggregates associated with cassiterite or phyllosilicates (Fig. 7B) shows that these grains are very frequent in samples spread across the study area.



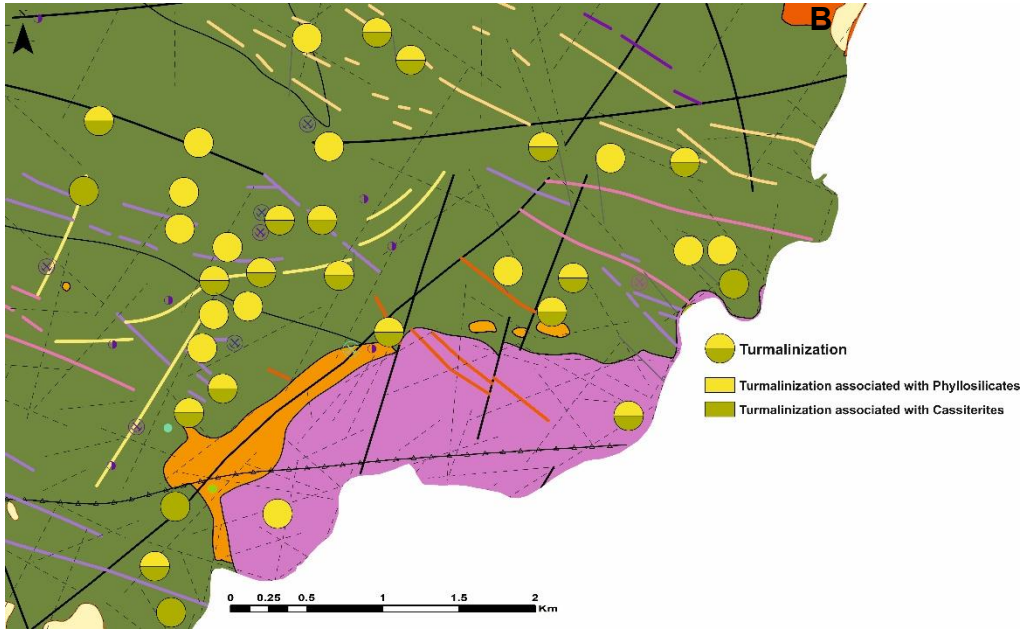
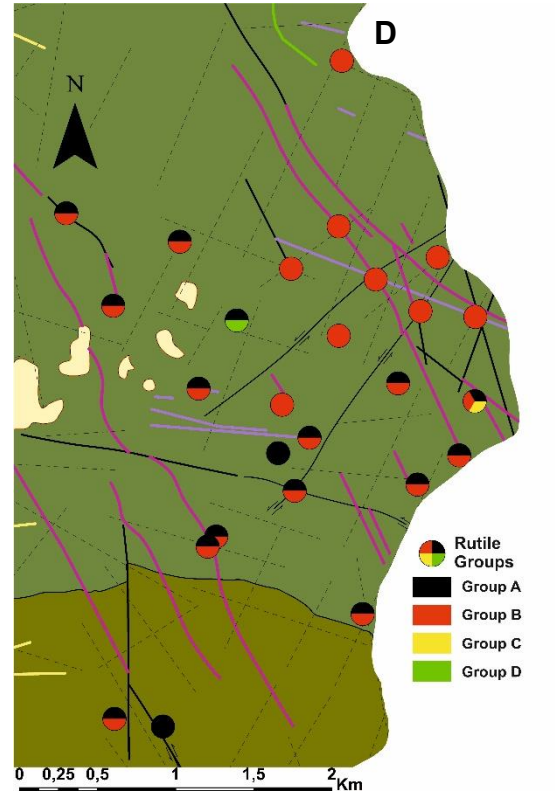
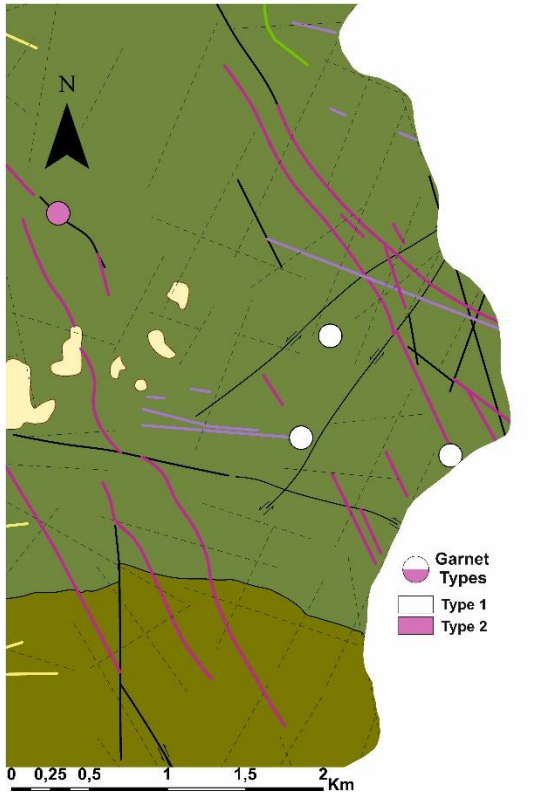
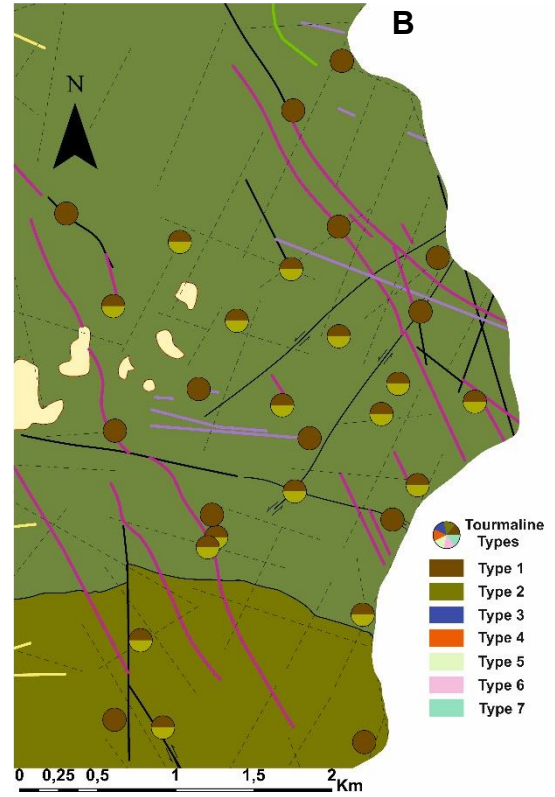
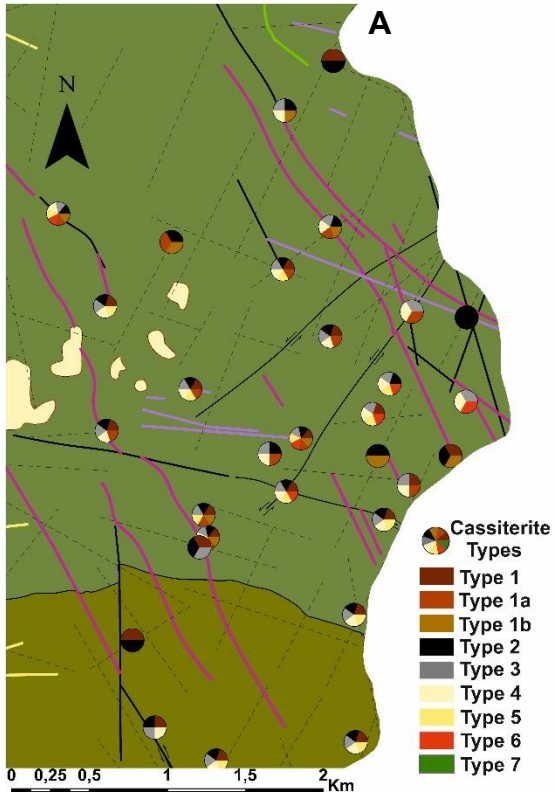


Fig. 7 - Maps of the regional distribution produced for Polygon 1: A) fresh and undifferentiated sulphide grains; B) tourmalinization: composite grains of fine tourmaline aggregates associated with cassiterite or phyllosilicates. (study of 69 alluvial samples; projected on an extract of the MOSTMEG geological map)

### 3.2.2.2. Polygon 2

The distribution and the relative abundance maps of the different mineral populations (Fig. 8 and 9) reveal a notable degree of variability in the populations of cassiterite, rutile, Type 1 garnet, sulphides, and tourmalinization near the Spanish border, particularly in the vicinity of the Estorninos granite. Within this same region, there is a prevalence of Type 1, 2, and 3 cassiterite. Group B of anhedral rutile (highlighted in red in Fig. 9D) tends to dominate, particularly to the north, while prismatic rutile of Group A is prominent close to the border, facing the Estorninos granite. Within this specific polygon, the predominant mineral population, of brookite, anatase, tourmaline, and garnet are the Type 1.



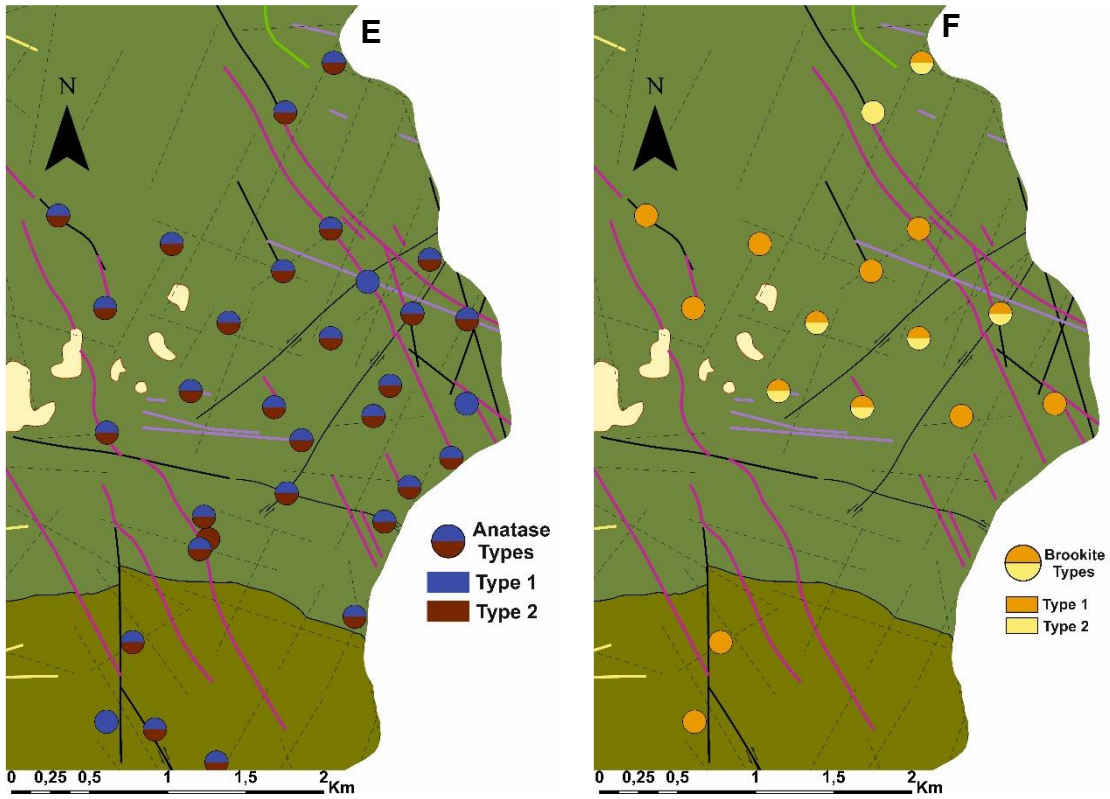
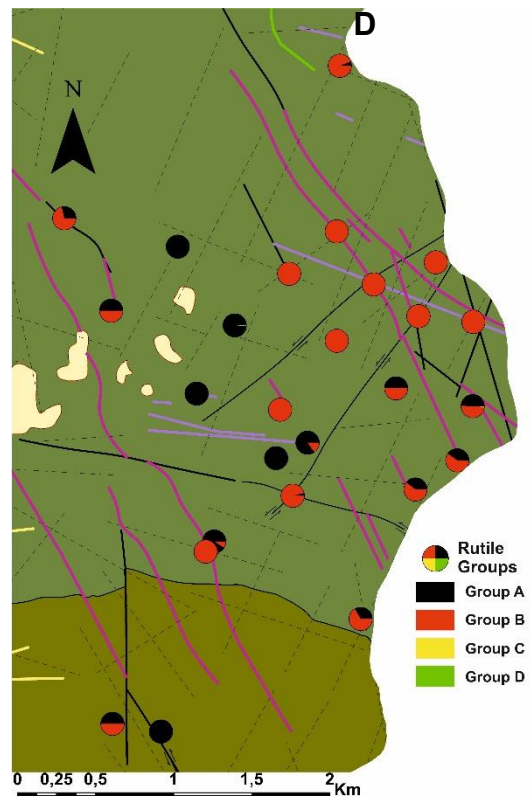
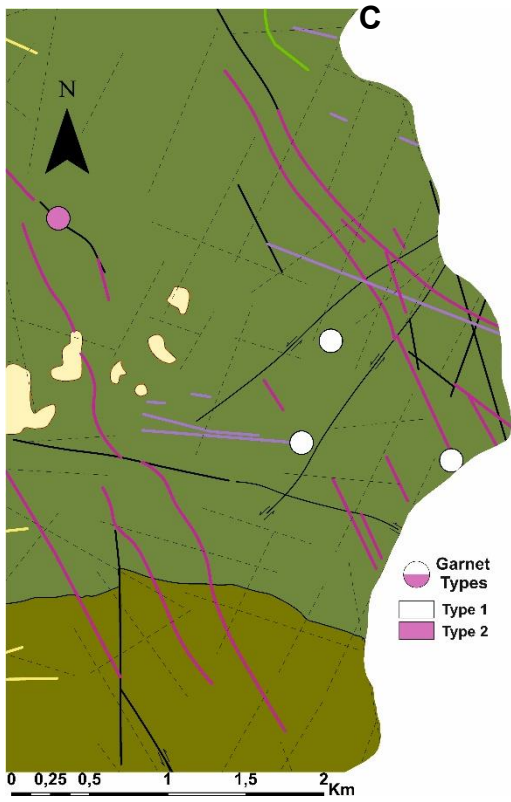
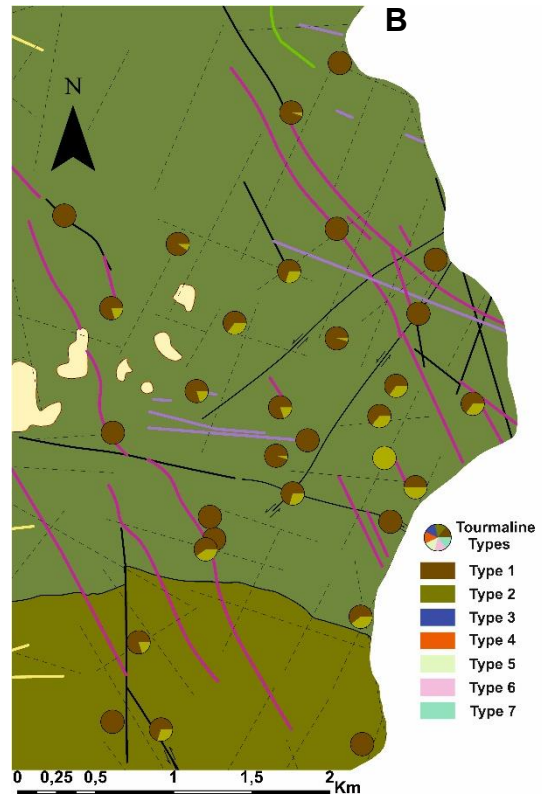
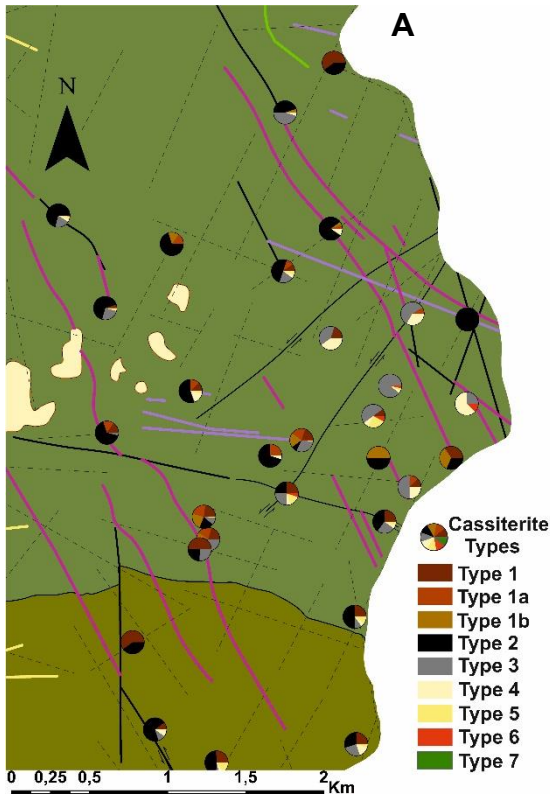


Fig. 8 - Maps of the regional distribution of mineral populations for Polygon 2 (35 samples) projected on an extract of the MOSTMEG geological map. Grain populations for: A) Cassiterite, defined mainly by color, diaphaneity and pleochroism; B) Tourmaline, mainly defined by color similar to legend markers; C) Garnet (defined by physical and chemical properties: Type 1: spessartine; Type 2: almandine); D) Rutile, defined by habit (Group A: prismatic; Group B: anhedral; Group C: acicular polycrystalline aggregates; Group D: bipyramidal and others undifferentiated); E) Anatase, defined by habit (Type 1: bipyramidal; Type 2: basal); F) Brookite, defined by color



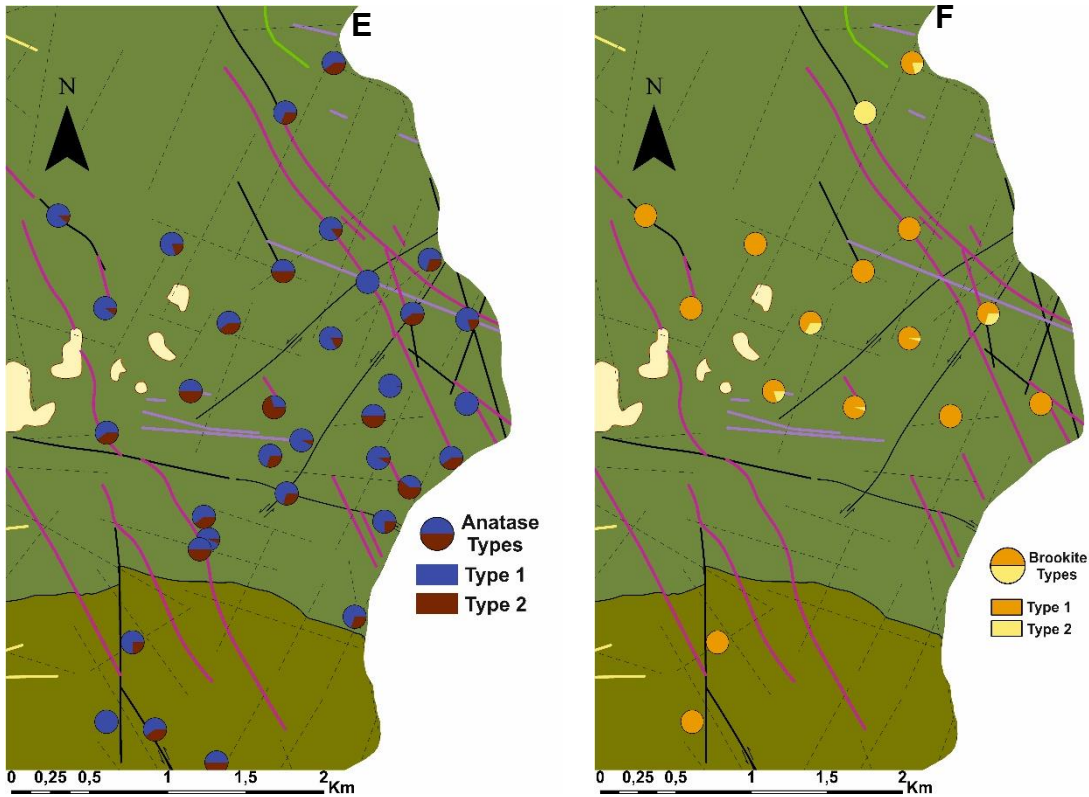


Fig. 9 - Maps of the relative abundance of mineral populations for Polygon 2 (35 samples) projected on an extract of the MOSTMEG geological map. Grain populations for: A) Cassiterite, defined mainly by color, diaphaneity and pleochroism; B) Tourmaline, mainly defined by color; C) Garnet (defined by physical and chemical properties: Type 1: spessartine; Type 2: almandine); D) Rutile, defined by habit (Group A: prismatic; Group B: anhedral; Group C: acicular polycrystalline aggregates; Group D: bipyramidal and others undifferentiated); E) Anatase, defined by habit (Type 1: bipyramidal; Type 2: basal); F) Brookite, defined by color

In the Polygon 2 area, the sulphides and tourmaline needles aggregates identified occur in samples near the Spanish border (Fig. 10A, B), where the isograds from the contact metamorphism from the Estorninos granite are still present according to Romão et al., (2010).

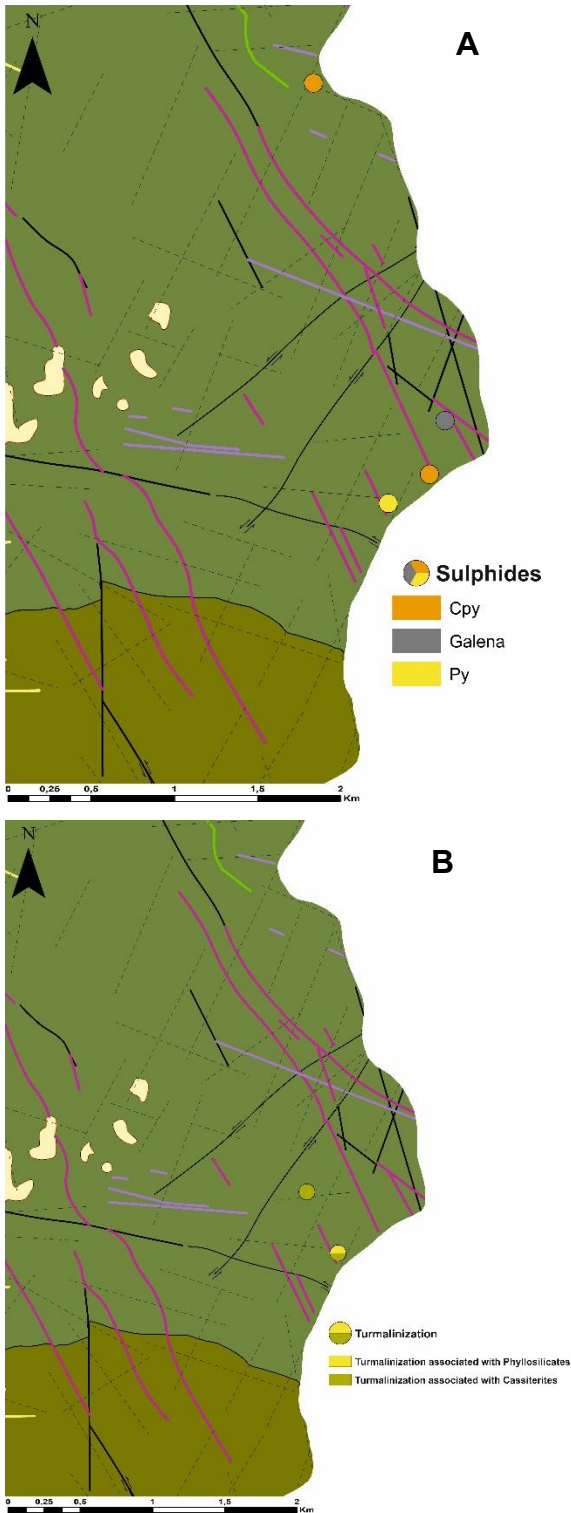


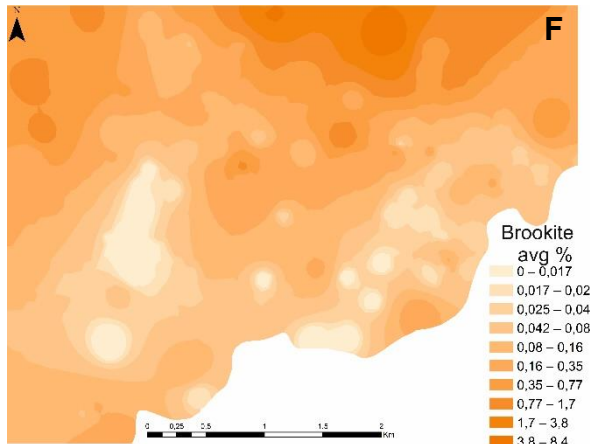
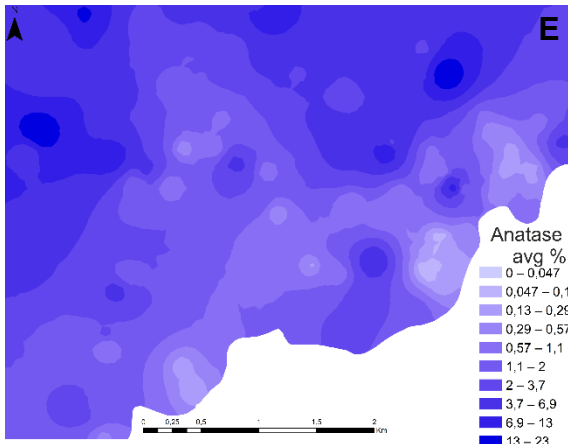
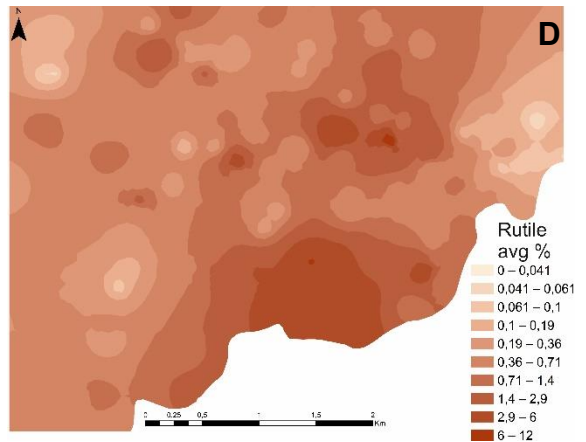
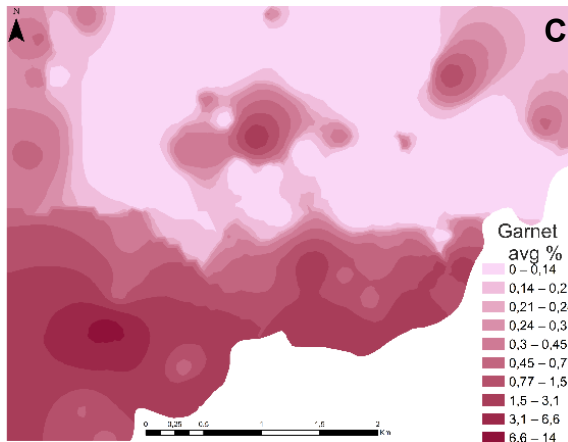
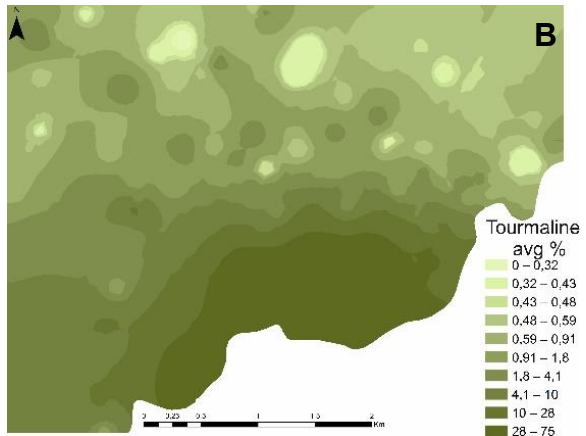
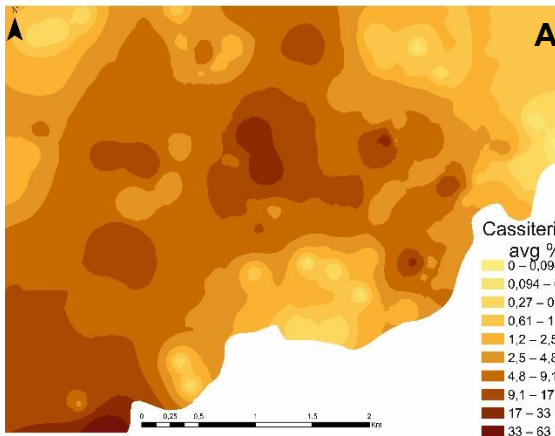
Fig. 10 - Maps of the regional distribution produced for Polygon 2: A) fresh sulphide grains; B) tourmalinization: composite grains of fine tourmaline aggregates associated with cassiterite or phyllosilicates; (study of 35 alluvial samples; projected on an extract of the MOSTMEG geological map).

### 3.2.3 Mineral abundance maps

In this section are presented the abundance distribution maps of the alluvial minerals of interest for this study, in the Polygon 1 and 2.

#### 3.2.3.1 Polygon 1

The presence of cassiterite is ubiquitous in the area of Polygon 1, with higher abundance near old exploration zones (see Fig. 1) and low abundance in granites of the Segura Massif (Fig. 11A). The alluvial wolframite becomes more abundant in the samples near the old mining works in W area of Polygon 1; three anomalies are identified, a northernmost one and two more anomalies aligned, approximately, NE-SW, in the area of the old exploration works (Fig. 11G). Regarding the scheelite grains, their abundance is relatively low; the samples with the higher scheelite abundance occur in the eastern area close to where the mineralized Sn-Li aplite-pegmatites outcrop and the Segura east granite border (Fig. 11H; see Fig. 1). In regard to the rutile abundance distribution map, it is possible to identify two zones with anomalous abundances, one in the zone where the granite outcrops and the other to the N of the granites where Sn-W, Pb-Ba mineralized and several barren veins outcrops (see Fig. 1), separated by a zone where the abundance of rutile is lower (Fig. 11D). Anatase is more abundant than rutile in this polygon, but it is also possible to identify two anomalous zones one on the W side and the other on the N side, despite some high values in the granite area (Fig. 11E; see Fig. 1). The brookite was the least abundant titanium polymorph identified in the studied samples, however a zone of anomalous brookite abundance is identified on the NE zone of Polygon1. In general, it is also possible to verify that both brookite and anatase abundances tend to increase with distance from the Segura massif (Fig. 11F). Tourmaline is more abundant in the Segura Massif and its exocontact rocks sourced samples, compared to the off-granite samples and its abundance tends to decrease in the samples further away from this massif (Fig. 11B). The garnet abundance is almost limited to the Segura Massif and its exocontact rocks, with very low abundances outside the granite influence and the maximum value of garnet was found in the samples collected near the muscovite granite outcrops (Fig. 11C; see Fig. 1).



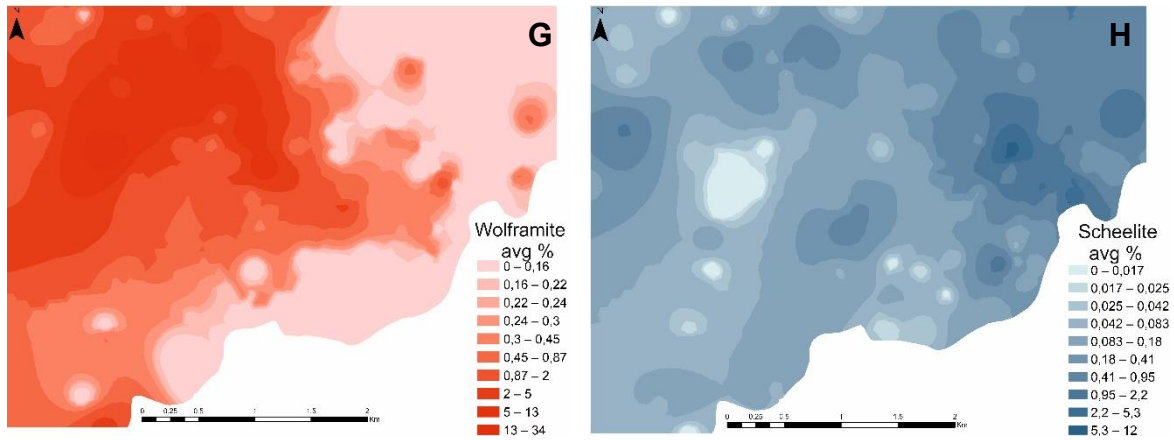
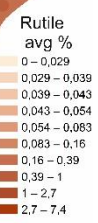
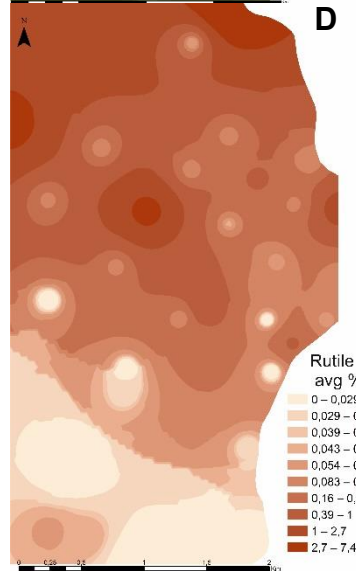
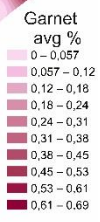
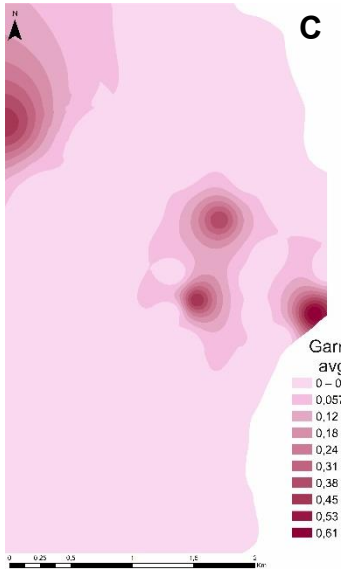
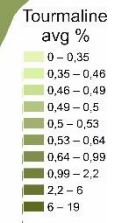
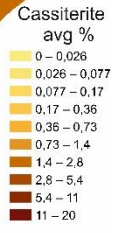
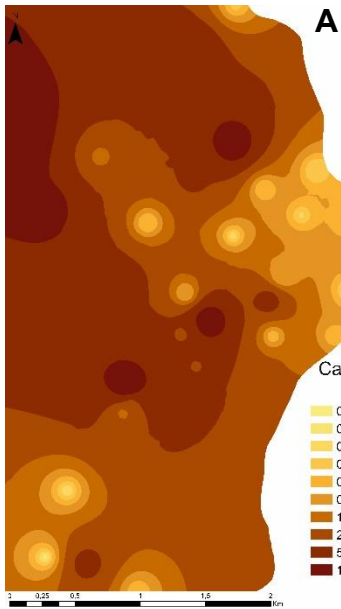


Fig. 11- Mineral distribution of the abundance of mineral grains of the heavy mineral samples in the Polygon1. A Cassiterite; B) Tourmaline; C) Garnet; D) Rutile; E) Anatase; F) Brookite; G) Wolframite; H) Scheelite.

### 3.2.3.2. Polygon 2

In the polygon 2 the abundances (Fig. 12) are, generally, lower for all minerals studied, the cassiterite with higher abundances are near the Cenozoic cover. The remaining area is somewhat ubiquitous in regards of cassiterite presence. The alluvial wolframite abundance in the Polygon 2 is very low, wolframite grains were only identified in 2 samples (Fig. 12G). The scheelite grains, on the other side, are ubiquitous in the samples near the Spanish border, nearby the zone that it's still affected by the contact metamorphism isograd from the Estorninos granite intrusion according to Romão et. al. (2010), with some samples having high concentrations of this mineral (Fig. 12H). Regarding the titanium polymorphs, rutile pattern is irregular but anatase and brookite seem to be more abundant in a zone which could be interpreted as an area further away from the influence of the Estorninos granite (in the southern part), and the Cabeza de Araya Batholith (in the north) intrusion, and in which other geological features occur, i.e. tectonic structures and several outcropping veins of different natures (Fig. 12D, 12E and 12F). Like in the Polygon 1, in Polygon 2 anatase is the most common titanium polymorph found in the samples. Tourmaline grains in the Polygon 2, are abundant in the samples near the Cenozoic cover, but also abundant in the northernmost samples, closer to the influence of the Cabeza de Araya Batholith, where tourmaline is usually abundant (Fig. 12B). On the other hand, the samples closer to the influence of the Estorninos granite are depleted in tourmalines grains. The garnet abundance in the Polygon 2 is very low; garnet grains were only identified in four samples in this area; however, the samples where garnet grains were found are on the same area were the highest concentration of scheelite grains was also found (Fig. 12C).



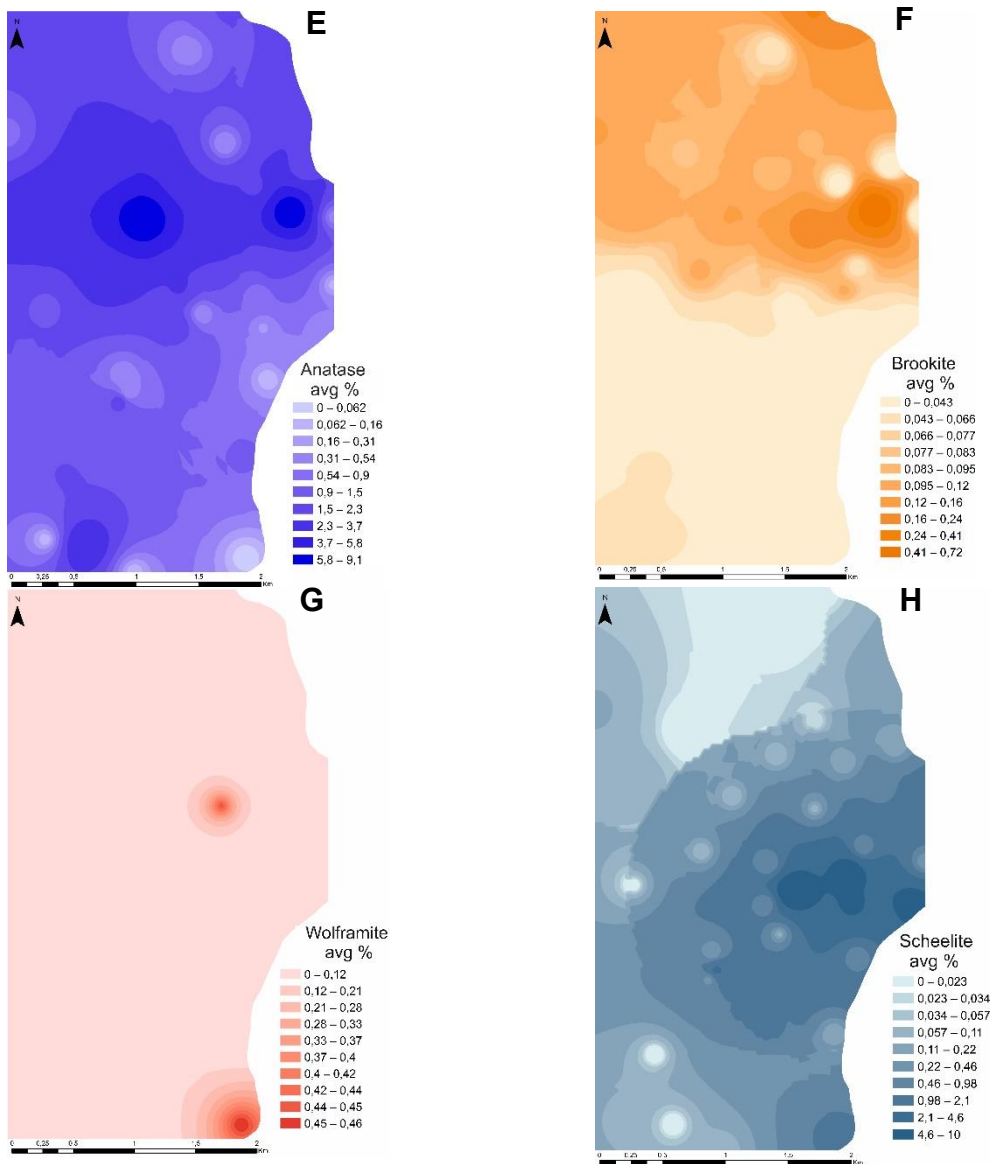
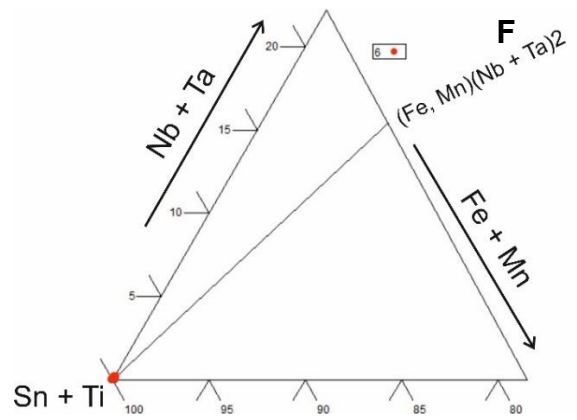
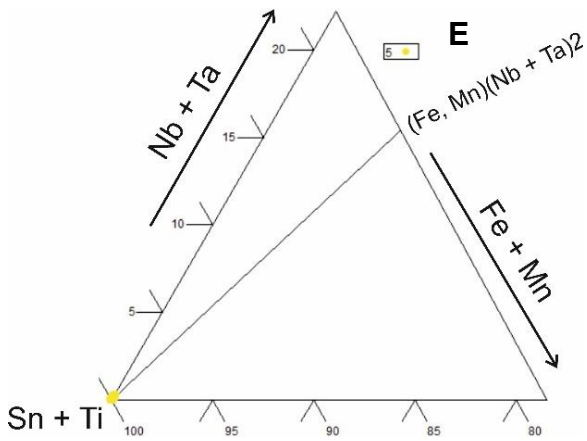
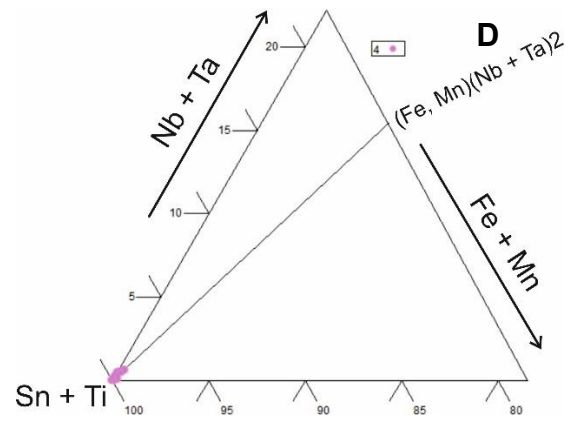
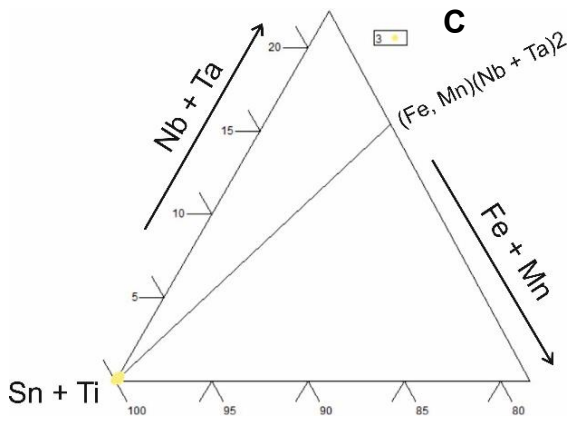
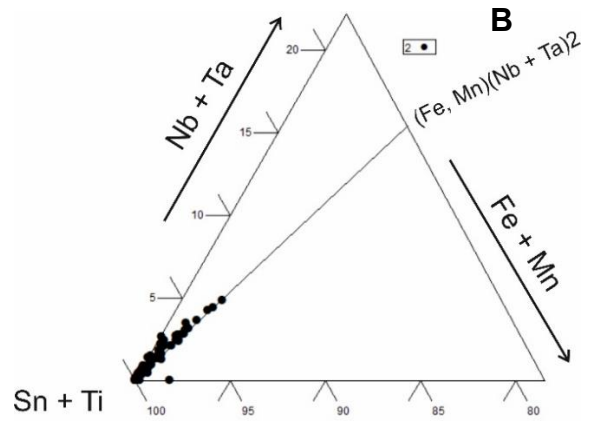
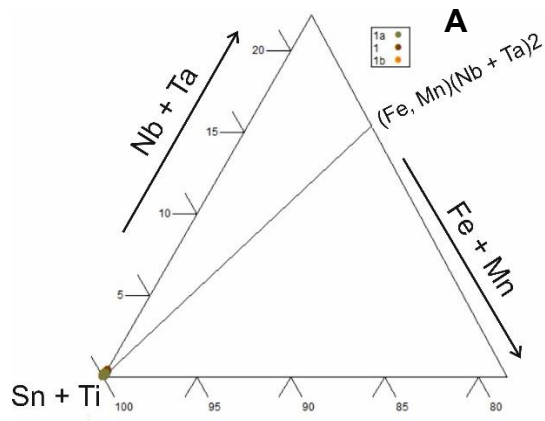


Fig. 12- Mineral distribution of the abundance of mineral grains of the heavy mineral samples in the Polygon2. A Cassiterite; B) Tourmaline; C) Garnet; D) Rutile; E) Anatase; F) Brookite; G) Wolframite; H) Scheelite.

### 3.3 Mineral Chemistry

From 435 chemical analysis performed, to date, on alluvial cassiterite grains via EMP, and 117 via LA-ICP-MS, the data allows some preliminary interpretations. In comparison with the composition of the alluvial cassiterite grains analyzed in the same region and presented by Grácio (2020), cassiterites studied under MOSTMEG are, in general, similar, except for the maximum contents in W and Fe. The maximum value of  $WO_3$  recorded in the cassiterite grains studied for this project (5.29 %  $WO_3$ ; EMP data) is higher than the value of the cassiterite grains analyzed in Grácio (2020; i.e., 1.93%  $WO_3$ ; EMP

data), the opposite happens with Fe (3.07 %, Grácio 2020; 0.74 %, this work; EMP data). The composition of the different cassiterite populations was projected on the triangular diagram (Sn+Ti)-(Nb+Ta)-(Fe+Mn) (Fig. 13), like it was done for the cassiterite data from Grácio 2020 where two distinct trends were identified, that may indicate two different sources for the cassiterite grains: a main trend that follows, in general, the columbo-tantalite substitution ( $3\text{Sn}^{4+} = 2(\text{Nb}^{5+}, \text{Ta}^{5+}) + (\text{Mn}^{2+}, \text{Fe}^{2+})$ ); and also a trend that indicates an excess of Nb+Ta in the cassiterite structure, suggesting cationic voids and/or the presence of Nb+Ta in the tetravalent state. The ternary diagrams from EMP and LA-ICP-MS analysis show that only the Type 2 cassiterite grains show considerable incorporation of trace elements (Fig. 13B and 13H), although the identification of the two substitution trends is not as evident as in the cassiterite grains from Grácio 2020 (additional cassiterite grains from samples, 295-493 and 295-491 near the ones where the cassiterite grains from Grácio (2020) showed the different substitution trend were handpicked for future analysis). The other cassiterite Types are almost pure cassiterite.



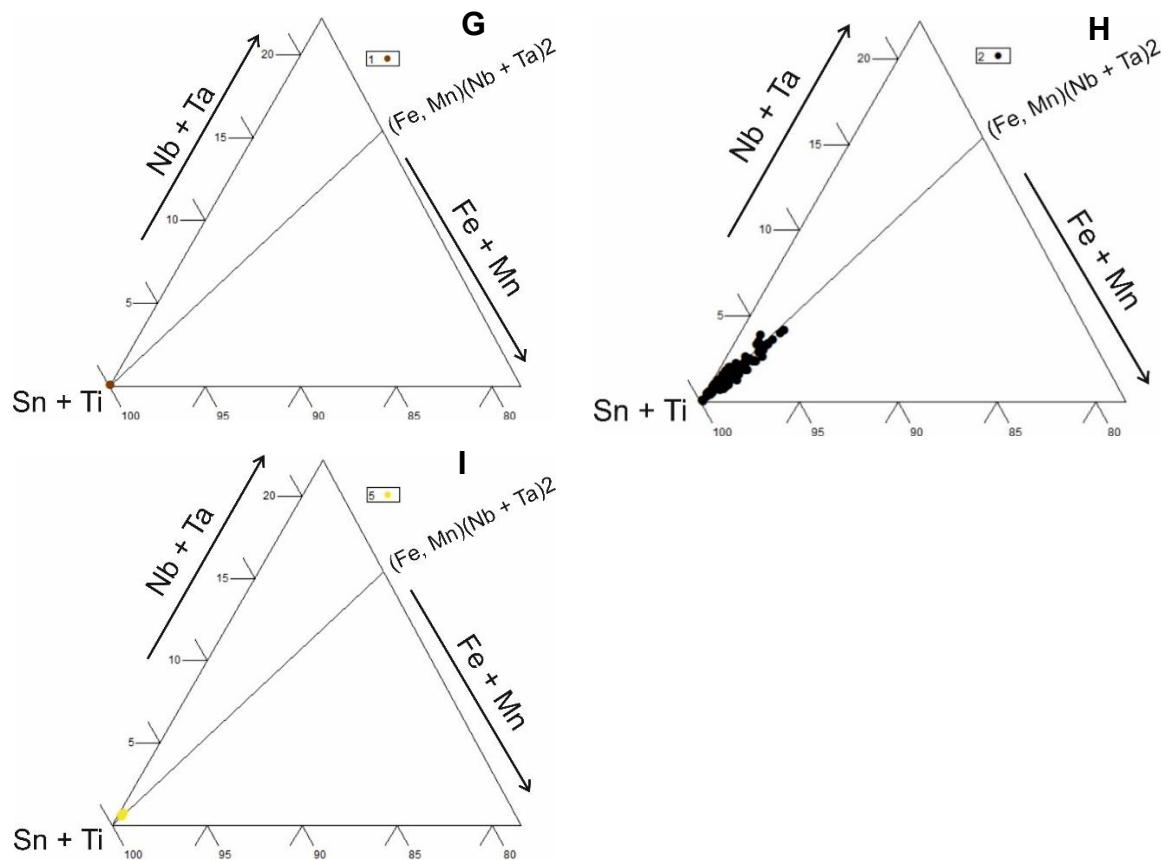
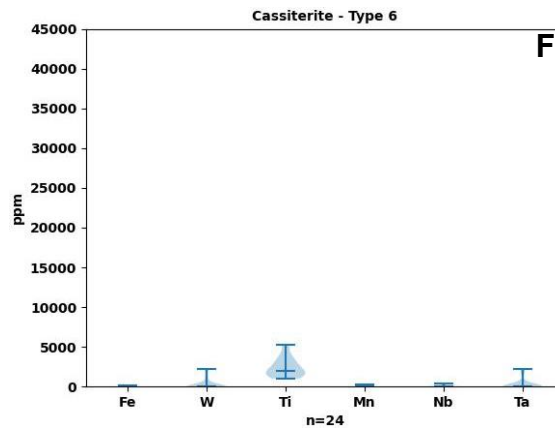
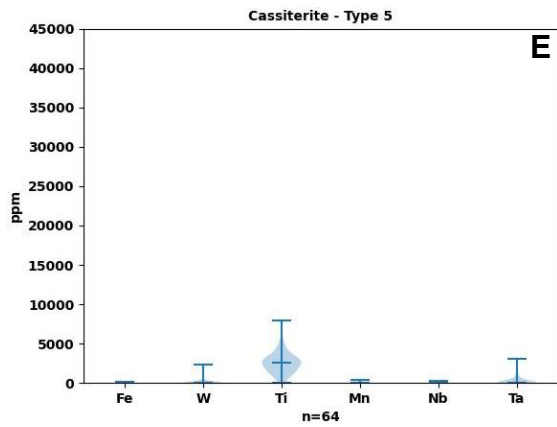
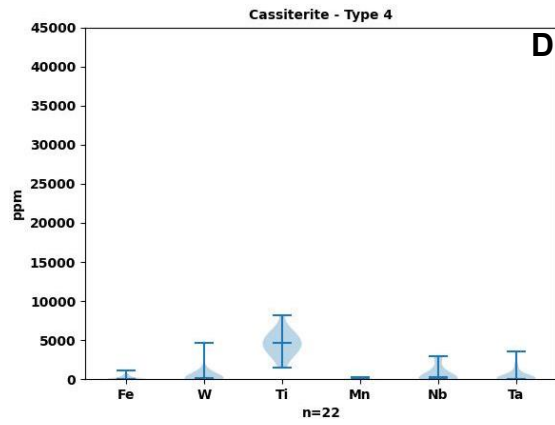
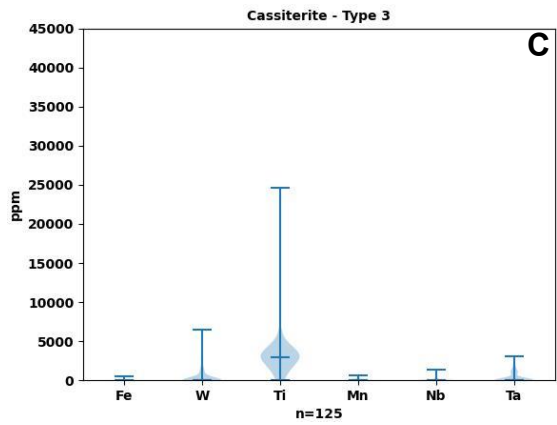
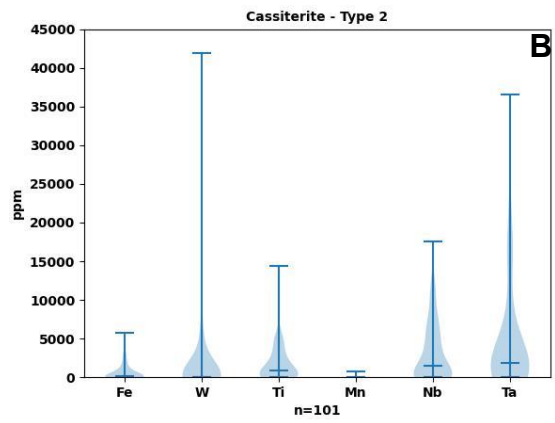
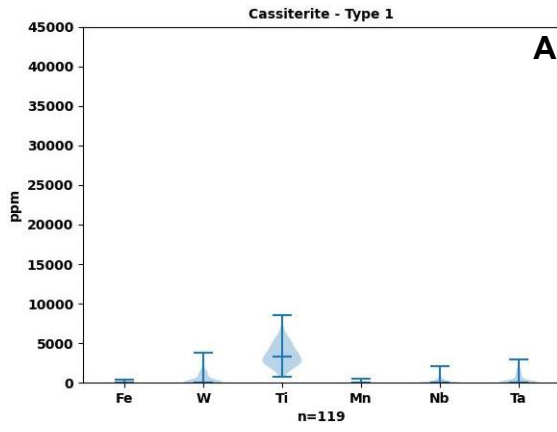


Fig. 13- Projection of the different population types of cassiterite grains analyzed in the alluvial samples of the Segura mining region, in the triangular diagram (Nb+Ta)-(Sn+Ti)-(Fe+Mn) by EMP: A) Type 1; B) Type 2; C) Type 3; D) Type 4; E) Type 5; F) Type 6. Projection of the different population types of cassiterite grains analyzed in the samples of alluvial heavy minerals of the Segura mining region, in the triangular diagram (Nb+Ta)-(Sn+Ti)-(Fe+Mn) by LA-ICP-MS: G) Type 1; H) Type 2; I) Type 5.

Violin plots are a powerful and versatile visualization tool by incorporating frequency distribution of data (concentration of trace element) into the typical statistical box plot, providing a more comprehensive view of the data. Violin plots were produced for each cassiterite type (Fig. 14). As shown by the ternary diagrams, Type 2 cassiterite grains analyzed by EMP and LA-ICP-MS have the highest trace element contents. These Type 2 cassiterite are the only cassiterite type analyzed where Ti is not the most abundant trace element, showing also high contents of W, Nb and Ta. The trace element fingerprint obtained by LA-ICP-MS is similar to the EMP analytical data except for the Type 5 cassiterite where a limited amount of LA-ICP-MS analysis were done.



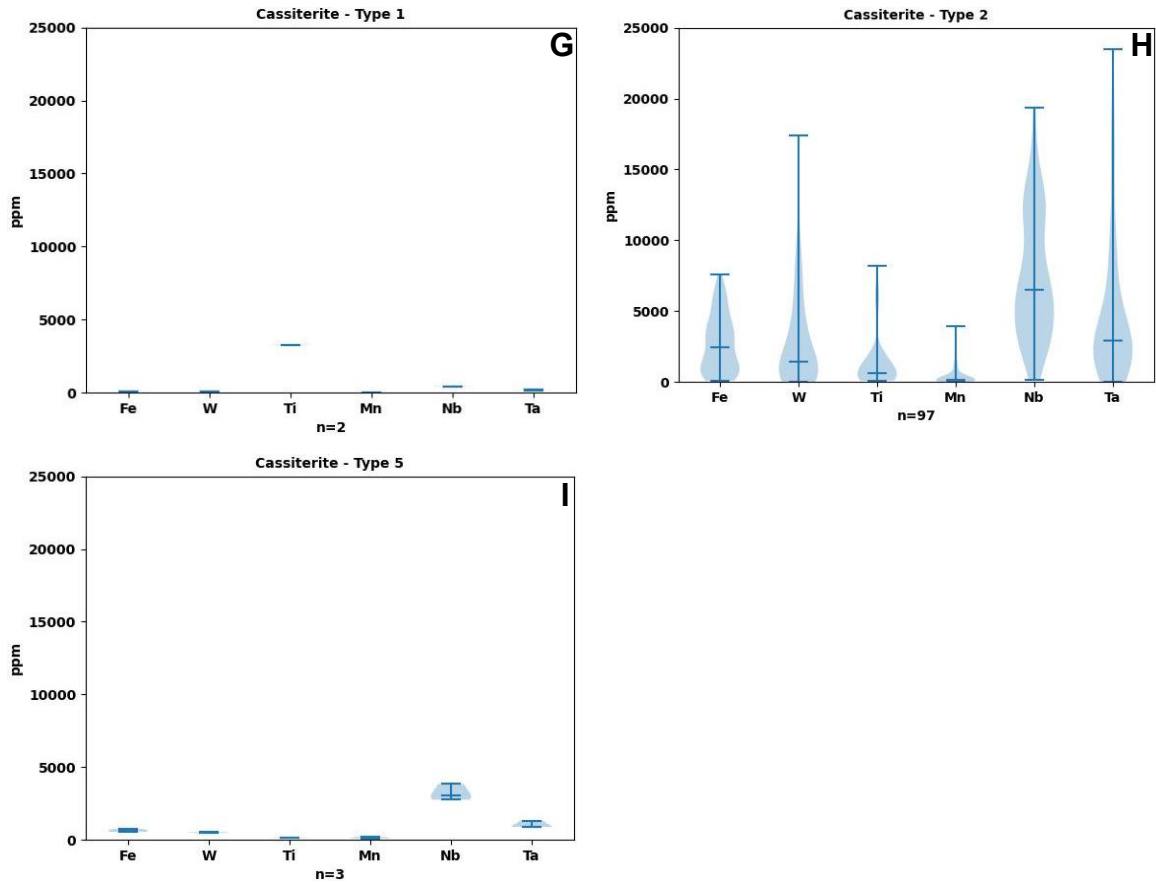


Fig. 14 – Violin Plots for the concentration of different trace elements in different cassiterite population types analyzed by EMP: A) Type 1; B) Type 2; C) Type 3; D) Type 4; E) Type 5; F) Type 6. Violin Plots for the concentration of different trace elements in different cassiterite types analyzed by LA-ICP-MS: G) Type 1; H) Type 2; I) Type 5.

Preliminary chemical data, obtained by LA-ICP-MS analysis (by FCUL MOSTMEG Partner), of alluvial tourmaline composition suggest the co-existence of 3 main compositional trends, Sn-enrichment, Sn+Li-enrichment and Li-enrichment (Fig. 15), creating reasonable expectations on their use as vectors to ore-forming systems, after an improved critical data analysis. The discrimination of the tourmaline types was now added by the grant holder to allow a better understanding of the results.

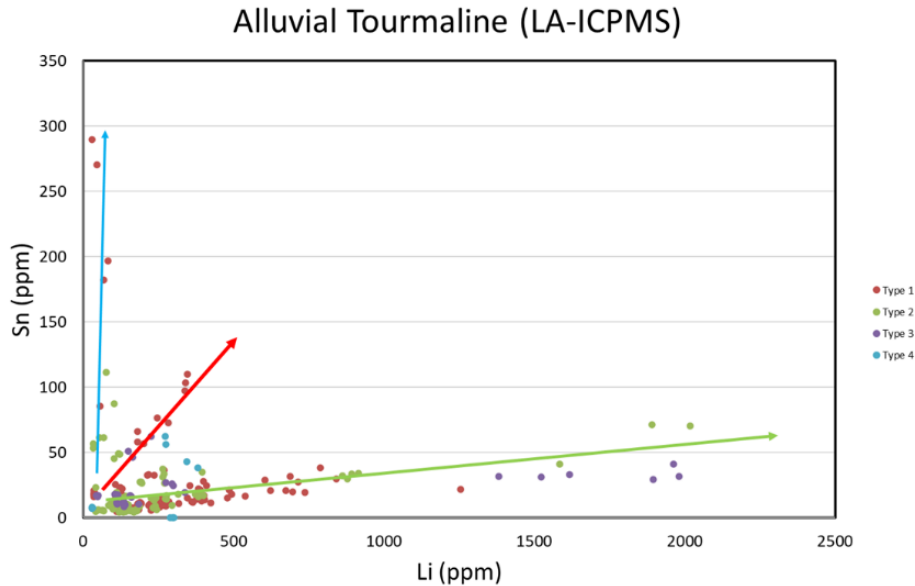


Fig. 15 - Sn vs Li diagram for alluvial tourmaline Types 1, 2, 3 and 4 from the Segura mining region (Polygon 1), showing the trends according to Sn-enrichment, Sn+Li-enrichment and Li-enrichment (updated from MOSTMEG 2<sup>nd</sup> Annual Progress Report).

The trace element contents in the TiO<sub>2</sub> oxides analyzed in MOSTMEG are comparable but slightly lower than those presented in Grácio (2020) and Gaspar et al. (2022), showing typical signatures of mineralization, more so in rutile than anatase. The few exceptions include: maximum V content in anatase [Max V in anatase grains from Grácio (2020): 5289 ppm; Max V in anatase grains from MOSTMEG project: 5819 ppm; EPM data], average and median Nb content in the anatase (average and median Nb in anatase grains from Grácio (2020) of: 1575 ppm and 1139 ppm, respectively; average and median Nb in anatase grains from the MOSTMEG project, of 2226 ppm and 1845 ppm, respectively). In order to visualize the relationship of the rutile with base metal deposits and Au Clark and Williams-Jones (2004) developed a triangular discriminant diagram used to distinguish between rutile signatures of mineralized and non-mineralized samples, with the vertices defined by Ti concentration values, 100(Fe+Cr+V) and 1000(Sn+W), in atoms per unit formula (apfu), as presented in Fig. 16. Most of the rutile from rocks unaffected by the hydrothermal mineralizing system project along, or close to, the Ti-(Fe+Cr+V) axis (Clark and Williams-Jones, 2004), whereas the rutile grains associated with metamorphic/metasedimentary processes tend to approach the Sn+W. These diagrams were used for both the rutile and the anatase analyzed in MOSTMEG (Fig. 16). Even with a smaller volume of chemical data it is possible to verify in Fig. 16, as shown in Grácio (2020) and Gaspar (2022), that the extension of the substitutions in the anatase, and therefore the incorporation of trace

elements in its structure is smaller than in rutile. The presence of grains with compositions that plot on the zones related with ore processes and on the zone related with metamorphic/metasedimentary processes shows the rutile grains of Group B have multiple sources, even within the same sample. In the case of the Ti oxides studied so far, it was not possible to establish a link between the populations identified and their chemical compositions, as is the case of cassiterites (Type 2). However, it is noteworthy that the most abnormal values of trace elements in anatase and rutile (Group B) correspond to grains collected from samples located close to mineralized bodies (i.e., sample 295-424, Ba-Pb Mineralized quartz veins; sample 295-85, Sn-W Mineralized quartz veins; sample 295-445, Sn-W Mineralized quartz veins). Anatase grains analyzed by LA-ICP-MS show the same enrichment towards the Sn+W vertex but also a preference towards the Fe+Cr+V vertex for some Type 1 anatase grains, not visible in the EMP analysis because of the higher detection limits (Fig. 16E). This preference is one more evidence for multiple sources of the anatase grains in these samples showing that the difficulty in determining their origin, can be overcome by the combination of the different physical and chemical characteristics.

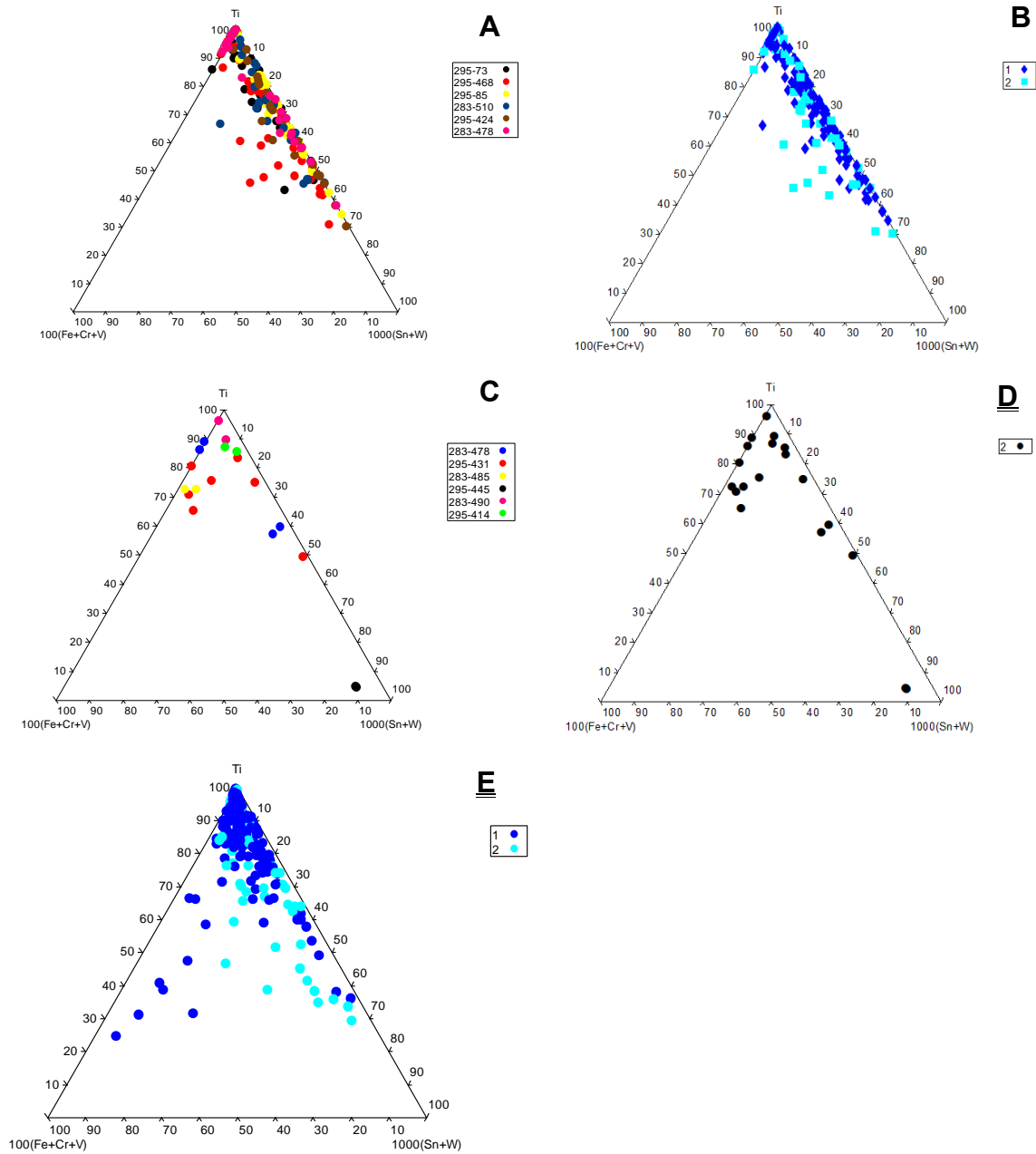


Fig. 16 - Discriminatory diagrams  $Ti+Fe+Cr+V+Sn+W$ , adapted from Clark and Williams-Jones (2004), for alluvial anatase and rutile from Segura Mining Region (Polygon 1): A) anatase grains discriminated by samples; B) anatase grains population Type 1 and 2, C), rutile grains discriminated by samples ; D) rutile grains Group B; E) anatase grains population Type 1 and 2, (LA-ICP-MS data),

As presented in the 2<sup>nd</sup> Annual report, the regional distribution, mineralogical and chemical preliminary data gathered for Type 1 and 2 garnet grains (Fig. 17A) show a positive correlation with the Mn-enriched spessartine observed in the contact metamorphic aureole contiguous to the Salvaterra do Extremo granite (to the north of Segura) and with the almandine found in Garnet-Cordierite Granite

Porphyry dykes related to the Cabeza de Araya batholith (in Spain), the southeastern extension of the Segura granite, respectively.

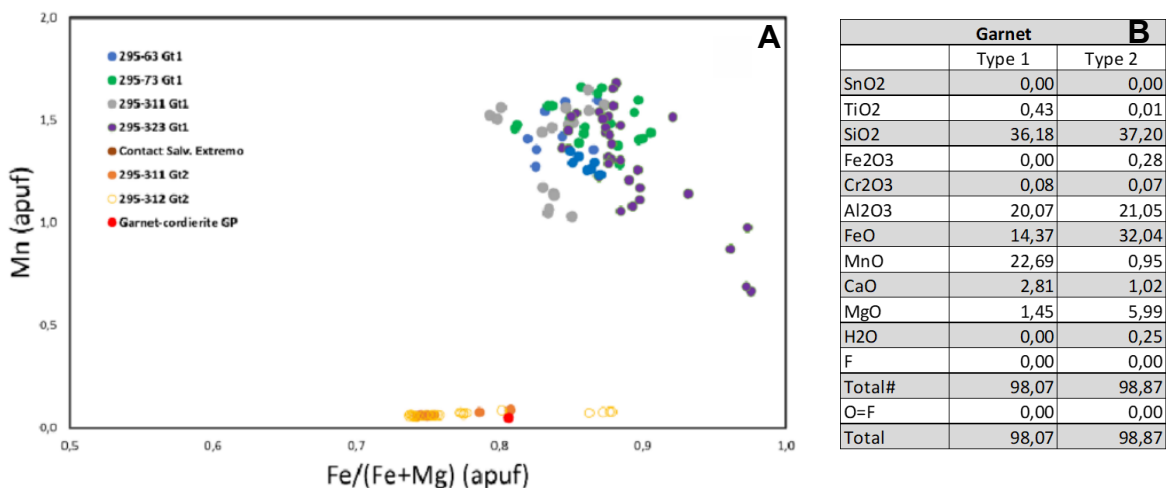


Fig. 17- A) Mn vs Fe/(Fe+Mg) diagram for alluvial garnet populations (Gt1: Type 1, spessartine; Gt2: type 2, almandine) from Segura. Spessartine data from contact metamorphism halo metasedimentary rocks in adjacent Salvaterra do Extremo region (to N of Segura) and almandine data from Garnet-Cordierite Granite Porphyry dyke associated with Cabeza de Araya batholith (Spanish territory; Corretgé and Suárez, 1994), were also plotted, showing positive correlation with alluvial garnet Type 1 and 2 from Segura, respectively (from MOSTMEG 2<sup>nd</sup> annual Progress Report). B) EMP analysis of a garnet type 1 (295-63) and type 2 (295-311).

## 4 Scientific collaboration and Publications

During the time under consideration (18 months), the grant holder has participated in several presential and online meetings with the MOSTMEG partners (transnational project), mainly in the context of the organization and development of Task 4.3 activities, including working with them in FCUL and Hércules Laboratory facilities, but also in the 2<sup>nd</sup> Annual meeting MOSTMEG (Transactional Project; September 4, 2022) with the other MOSTMEG Transnational project partners. Moreover, he has submitted a Short Activities Report with the Research Grant extension request, contributed to the production of the 2<sup>nd</sup> and 3<sup>rd</sup> Annual Progress report (2022 and 2023, respectively), and his work will contribute to the Deliverable D. 4.3. Regarding scientific publications, he has participated as coauthor in one scientific paper (with LNEG, FCUL and Hércules Laboratory) and one abstract (with LNEG and FCUL):

Gaspar, M. **Grácio**, N. Sagueiro, R. Costa, M., 2022. Trace Element Geochemistry of Alluvial TiO<sub>2</sub> Polymorphs as a Proxy for Sn and W Deposits. *Minerals*, 12, 1248. <https://doi.org/10.3390/min12091067> (see attached).

**Salgueiro, R.**, Grácio, N., Gaspar, M., de Oliveira, D., 2023. Alluvial Sn and W minerals mapping for mineral resources exploration and research in Segura mining region (Portugal). XI Congresso Nacional de Geologia - Livro de Resumos; Coordenadores da Edição: F.C. Lopes, P.A. Dinis, L.V. Duarte, P.P. Cunha, Departamento de Ciências da Terra da Faculdade de Ciências e Tecnologia da Universidade de Coimbra. Coimbra 16-20 de julho, p. 415-416. ISBN: 978-989-98914-8-7; <https://xicng.net/wp-content/uploads/2023/07/XI-CNG-2023-Livro-Resumos.pdf> (see attached).

Moreover, it is expected that his work will be part of future publications already under development, where he will be coauthor.

## 5. Final considerations

The work proposed in the workplan (Edital n.º14 and extension request, i.e. mineralogical study of alluvial heavy minerals, handpicking and production of mounts and chemical analyses and the associated data processing and interpretation (possible, to date) was completed. Due to LNEG, FCUL and Hercules internal constrains it wasn't possible to follow more chemical analysis. However, despite the constrains, in conclusion, the present study developed during the 18 months, successfully achieved the objectives with the identification and mineralogical characterization of the key minerals relevant to the project, accompanied by a semi-quantitative assessment of their respective percentages, recognizing particularities of alluvial heavy mineral associations from distinct sources and, in cases, their overlay. Further refinement of the research involved the implementation of a methodology to distinguish the various populations within cassiterite, titanium oxides, tourmaline, and garnet grains, with an additional experimental study that allowed to determine their (relative) semi-quantification. The generation of mineral distribution maps at a regional level offers a valuable means to approach and assess the potential source contributions to the alluvial samples even before the chemical analyses. The chemical data obtained and available showed that, at least, some cassiterites (and garnet) populations defined based on physical properties have distinct chemical characteristics; and most abnormal values of trace elements in some anatase and rutile populations seem to be related to the close occurrence of this minerals with mineralized bodies. The subsequent mineral chemical analyses hold the promise of clearly differentiating their source and verifying the possible correlations between the chemical and mineralogical populations.

Romão, J., Cunha, P.P., Pereira, A., Dias, R., Cabral, J., Ribeiro, A., (2010). Notícia Explicativa das Folhas 25-C; 25-D; 29-A Rosmaninhal Segura Retorta (Sector Norte). Laboratório de Energia e Geologia, Lisboa, 54 p.

This integrated approach enhances the understanding and evaluation of the alluvial samples and their origins in a comprehensive manner, augmenting the depth of the chemical characterization already conducted in MOSTMEG.

#### Acknowledgements

The research was supported by Fundação para a Ciência e Tecnologia, I.P. through national funds, by the MOSTMEG project (ERA-MIN/0005/2019): <http://doi.org/10.54499/ERA-MIN/0005/2019>, <http://mostmeg.rd.ciencias.ulisboa.pt/>

Alfragide, 15 December, 2023

*Nuno Miguel S. C. Grácio*  
Nuno Grácio

#### References

Clark, J. R., Williams-Jones, A. E., (2004). Rutile as a potential indicator mineral for metamorphosed metallic ore deposits. *Divex*, 7(Sous-projet SC-2), 17pp.

Corretgé, L.G., Suárez, O., (1994). A Garnet-Cordierite Granite Porphyry Containing Rapakivi Feldspars in the Cabeza de Araya Batholith (Extremadura, Spanish Hercynian Belt). *Mineralogy and Petrology*, 50, pp. 97-111.

Gaspar, M., Grácio, N., Salgueiro, R., Costa, M., (2022). Trace Element Geochemistry of Alluvial TiO<sub>2</sub> Polymorphs as a Proxy for Sn and W Deposits. *Minerals*, 12, 1248. <https://doi.org/10.3390/min12091067>

Grácio, N., (2020). Caracterização mineralométrica e química de minerais pesados aluvionares: aplicação à prospeção de Sn e W na região de Segura. Relatório de estágio de mestrado, *Geologia Económica (Prospeção mineral)* Universidade de Lisboa, Faculdade de Ciências, 67 p. <http://hdl.handle.net/10451/45362>

Parfenoff, A., Pomerol, C., Tourend, J., 1970. *Les minéraux en grains*, Masson et Cie editeurs 571 p.

Mapa metalogenético de la provincia de Cáceres Escala 1:200.000 (2006). Instituto Geológico y Minero de España: Junta de Extremadura. Dirección General de Ordenación Industrial, Energía y Minas-Madrid: Instituto Geológico y Minero de España